NASA/USRA ADVANCED DESIGN PROGRAM

Final Report 1987-1988

THE HORIZON

A Blended Wing Aircraft Configuration

Design Project

Design Team Members:

Paul Keidel Project Leader
Mark Gonda
Damon Freeman
Jay Kim
Yul Hsu

CALIFORNIA STATE POLYTECHNIC UNIVERSITY POMONA
Aerospace Engineering Department

Table of Contents

List of Symbols

A_c - intake capture area

A_e - nozzle exit area

C - local thermal conductivity constant

C_D - drag coefficient

C_{Dq} - drag change with pitch rate

C_{Du} - drag change with speed

C_{D0} - zero lift drag coefficient

C_{D0} - zero lift drag coefficient

$C_{D\alpha}$ - drag change with angle of attack

$C_{D\alpha}$ - drag change with angle of attack rate

C_L - lift coefficient

$C_{L\,max}$ - maximum lift coefficient

C_{LB} - break lift coefficient

C_{Lq} - lift change with pitch rate

C_{Lu} - lift change with speed

$C_{L\alpha}$ - lift change with angle of attack

$C_{L\dot{\alpha}}$ - lift change with angle of attack rate

C_{Txu} - thrust coefficient change with speed

C_a - nozzle losses due to flow angularity

C_{fg} - nozzle thrust coefficient

C_{macWB} - mean aerodynamic center:wingbody

C_{mq} - pitching moment change with pitch rate

C_{mu} - pitching moment change with speed

$C_{m\alpha}$ - pitching moment change with

$C_{m\dot{\alpha}}$ - pitching moment change with pitch rate

C_{lp} - rolling moment change with roll rate

C_{lr} - rolling moment change with yaw rate

$C_{l\beta}$ - rolling moment change with sideslip

C_{np} - yawing moment change with roll rate

C_{nr} - yawing moment change with yaw rate

$C_{n\beta}$ - yawing moment change with sideslip

C_{p0} - specific heat of freestream

C_{p4} - specific heat of gas generator

C_v - nozzle friction losses

C_{yp} - side force change with roll rate

C_{yr} - side force change with yaw rate

$C_{y\beta}$ - side force change with sideslip

C_1 - vortex lift constant, conductivity const

C_2 - thermal conductivity constant

D - drag

D_{reqd} - required engine diameter

D_1 - engine diameter at analysis

E - energy rate emission

F - engine thrust force

F_{ram} - ram drag force

I - specific impulse

K_B - break constant

K' - constant based on Oswald efficiency

L - convection flow length

L_H - length from cg to horizontal ac

L_{WB} - length of wing body

M - Mach number

M_0 - freestream Mach number

M_4 - gas generator exit Mach number

Nu^* - Nusselt number

P_i - nozzle inlet pressure

Pr - Prandtl Number

P_0 - freestream static pressure

P_7 - freestream static pressure

R - gas constant of air, nose radius

Re^* - reference Reynolds Number

S - exposed wing area

S_A - airborne distance

S_B - breaking distance

S_{CL} - take off climb distance

S_{FR} - free roll distance

S_G - take off ground distance

S_R - take off rotation distance

S_{TR} - take off transition distance

T - thrust, freestream temperature

T_L - local temperature

T_{SL} - stagnation local temperature

T_{WS} - wall temperature

T_{aw} - adiabatic wall temperature

T_r - rolling mode, recovery temperature

T_{reqd} - thrust required

T_s - spiral mode, surface temperature

T_w - static wall temperature

T_{wf} - element final temperature

T_0 - static air temperature

T_1 - thrust at engine size analyzed

T_4 - rocket static exit temperature

T^* - reference temperature

U - forward speed

V_C - design cruise speed

V_{CL} - climb velocity

V_D - design diving speed

V_{TO} - takeoff velocity

V_a - design maneuvering speed

V_e - velocity of mass at nozzle exit

V_i - velocity of mass at nozzle inlet

V_{s1} - stall velocity

V_{50}	- velocity required to clear 50 ft obstacle	W	- weight
X_{acH}	- horizontal aerodynamic center	X_{acWB}	- wing-body aerodynamic center
X_{cg}	- center of gravity location	X_{mg}	- distance from point to center of mass
Z_D	- distance from point to drag axis	Z_T	- distance from point to thrust axis
Z_{mg}	- distance from point to center of mass	a_0	- freestream speed of sound
a_4	- gas generator speed of sound	c	- mean chord
h	- fuel heating rate, heat transfer coefficent	g	- gravity
g_c	- Newton's constant	k	- thermal conductivity
k_{32}	- thermal conductivity constant	k^*	- reference thermal conductivity
l	- wing length	m	- mass
m_e	- nozzle exit mass flow rate	m_f	- fuel mass flow rate
m_0	- freestream mass flow rate	m_4	- gas generator mass flow rate
p	- freestream pressure	p_L	- local pressure
p_{02}	- total pressure behind shock wave	$q_{T.O.R.}$	- dynamic pressure at rotation
q_{bl}	- convective heating rate	q_{rad}	- stagnation point radiation
q_s	- stagnation point heating rate	r	- recovery factor
s	- wing span	t_c	- skin thickness
ΔC_{fg}	- nozzle losses for leakage and cooling air	Δt	- time increment
Θ	- angle between velocity and surface	α	- bypass ratio
η_{spec}	- MIL specification total pressure recovery	δ	- wedge angle
ε	- emissivity	γ	- ratio of specific heat of air
θ_{CL}	- angle of climb	θ_{ab}	- bypass total/freestream static pressure
θ_{ar}	- rocket total/freestream static pressure	θ_0	- freestream total/freestream static pres
θ_4	- turbine total/rocket static pressure	μ_L	- local viscosity

σ - Stephan-Boltzman constant

τ - volume/area ratio

τ_c - bypass total/inlet total temperature

τ_f - burner total/inlet total temperature

ω_D - high frequency Dutch Roll

ω_{nph} - high frequency phugoid

ω_{nsp} - high frequency short period

ζ_D - low frequency Dutch Roll

ζ_{ph} - low frequency phugoid

ζ_{sp} - low frequency short period

1.0 INTRODUCTION

The need for a trans-Pacific air route has been established. Today's airlines are attempting to meet the demand that has been caused by increased trading in the Far East, but with the limitations of the conventional aircraft being used by the airlines, the demand is exceeding the supply. One solution that has been proposed is the use of hypersonic vehicles capable of crossing the pacific ocean in under three hours. The technology to build the individual components of such vehicles has been in existence for many years, however, the technology to integrate all of the components into one sound and practical vehicle are only now emerging. The High-Speed Civilian Transport (HSCT) is the result of merging the old and new technologies.

The HSCT is a Mach 2-5 transport aircraft. It is designed to compete directly with today's standard commercial aircraft. It is capable of taking-off and landing at existing airports, it seats over 200 passengers, first class amenities are available, and ticket prices are competitive. The HSCT caters to the business traveler. This is because the highest demand for the HSCT lies in this sector.

The study of the HSCT is divided into four groups according to planform configuration. This report concerns itself with the blended wing-body configuration. The joined wing, wave rider, and oblique planforms are studied in the other volumes.

2.0 REQUIREMENTS

2.1 Request for Proposal

The request for proposal(RFP) of the NASA/USRA Advanced Design Program which governed the Horizon design concerned a hypersonic civilian transport(HSCT). This RFP was decided upon by all four of the HSCT design groups, a decision based on the NASA funded HSCT studies conducted by McDonnell Douglas and Boeing Aircraft Companies. The vehicle's gross take-off weight was to be less than one million pounds and have a range of 6,500 nautical miles. It was to cruise at 100,000 feet at a speed between Mach 3 and Mach 6. The vehicle's performance was to allow it to operate from an 11,500 foot runway, constant with current metropolitan airport sizes, and carry between 200 and 250 passengers. FAR 25 states that fuel reserves be five percent of the total fuel on board, and as for noise, the ground overpressure of the HSCT aircraft must be less than one pound per square inch.

Not stated but implied in this RFP was a vehicle planform effects study. Horizon has a blended wing-body. The joined wing, oblique wing, and caret planforms were considered by the other HSCT design groups.

2.2 Mision Profile

The mission profile(MP) was also agreed upon by the four HSCT design groups, and is shown in Figure-2.1. As stated in the RFP, the total mission length of the Horizon HSCT is 6,500nm. The largest portion of this mission, 4,900nm, is maintained in the supersonic/hypersonic cruise mode. This cruise is held at

100,000ft to meet FAR 25 noise requirements. Climb to cruise involves two major steps. Subsonic flight speeds would be maintained until the vehicle is clear of large land masses and other traffic, possibly up to 45,000ft. Once clear, a supersonic climb between Mach 1 and Mach 3 would be initiated to reach the cruising altitude where three quarters of the mission (length) will take place.

During the descent at the end of the cruise, the vehicle must decelerate to a speed just below Mach 1 before crossing over land, again due to noise restrictions and to ensure a safe entry into the respective Terminal Control Area(TCA). A loiter time of one half hour, in terms of fuel, is included in the descent for delays due to traffic. And pending future changes in current landing approaches, the Horizon's approach flight phase may cover up to 200nm. With respect to the Mission Profile figure, the five percent of fuel reserves are shown as a separate mission after landing.

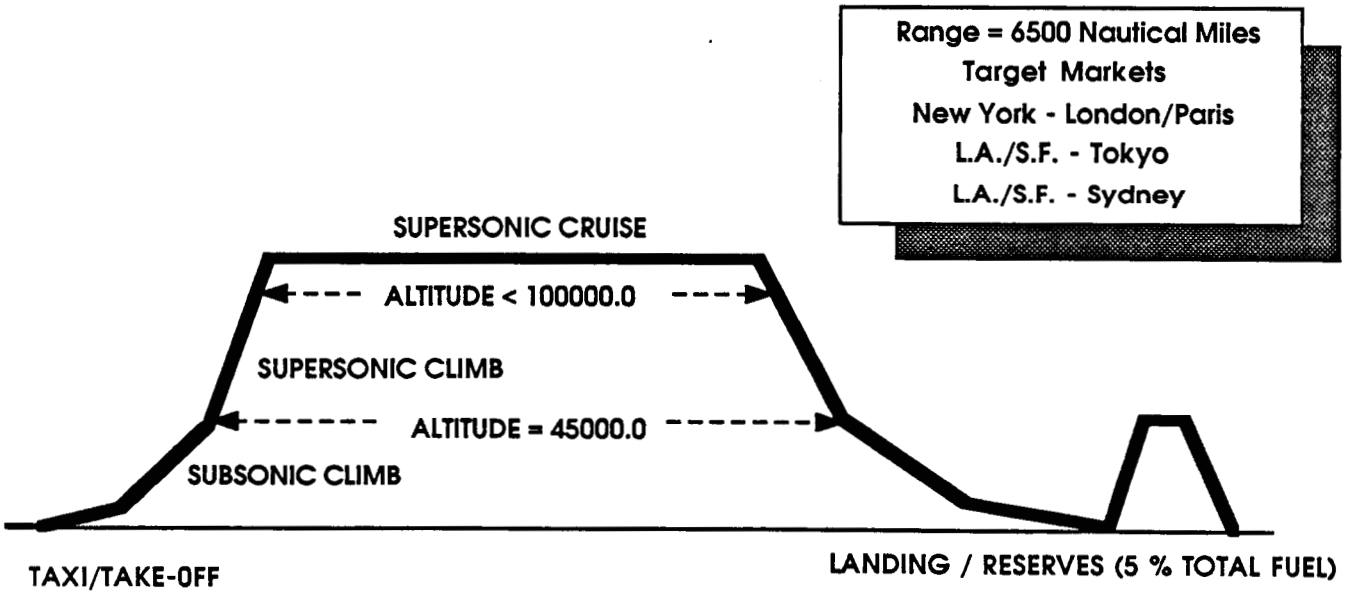

3.0 SIZING - CONFIGURATION

3.1 INITIAL SIZING OF THE AIRCRAFT

The initial sizing of the aircraft was based on the original Request For Proposal (RFP) that stipulated the aircraft mission requirements. This mission requirement estimated one million pound (1M) gross take-off weight and the take off/landing distance to be contained within already existing airfields in the target markets. Based on this information, the sizing plot was constructed by utilizing Roskam's and Nicolai's [Reference 1 & 2] equations and the sizing plot is shown on figure-3.1

3.1.1 TAKE-OFF DISTANCE SIZING

Since our target markets are located in metropolitan coastal cites, and our flight requirements can only be met to a specified field length, serving only to predetermined cities, avoiding any flight that is considered supersonic over large portions of land, we do not have any possible emergency situations that would requires the aircraft to land on a runway located in high altitude airport. The sizing consideration requirements are optimized for the sea-level conditions plus five degrees (5°R). The general equation (Roskam) used to evaluate the take-off distance (S_{TO}) is,

$$(3.1)\quad S_{TO} = \frac{k\,(\frac{W}{S})}{\sigma C_{L_{max}}\,(\frac{T}{W})} \qquad \sigma = \frac{(\frac{P}{P_{SL_{std}}})}{(\frac{T}{T_{SL_{std}}})} \qquad k = \frac{1}{AR\,\pi\,e}$$

where $C_{L_{max}}$ is the take-off maximum lift coefficient value. For our purposes, equation 3.1 was re-arranged to yield required $(\frac{T}{W})$ based on assumed $(\frac{W}{S})$ values from estimated $C_{L_{max}}$ values. The estimate values used for these calculations were taken from other aircrafts of the similar sizes. Though we did not look at any high altitude take-off requirements, we did however evaluated a hot-day and a cold-day requirements.

3.1.2 LANDING DISTANCE SIZING

For the reasons cited in 3.1.1, landing requirements were also evaluated under the similar considerations. The general equation used for this analysis was taken from Nicolai given by equation 3.2 solving for the required distance S_L,

$$(3.2) \quad S_L = \frac{118\,(\frac{W}{S})}{\sigma\, C_{L_{max}}} + 400$$

where $C_{L_{max}}$ is maximum landing lift coefficient value. Again, like equation 3.1, this equation too was re-arranged to yield required $(\frac{W}{S})$ for estimated $C_{L_{max}}$ values.

3.1.3 CRUISE SPEED SIZING

For initial cruise sizing consideration, we assumed a value for C_{D_o} for our cruise speed range between Mach 3 to 6 as stipulated in the RFP. By assuming a value for these Mach numbers, and using a drag equation (see Chapter-5), the $(\frac{T}{W})$ required was evaluated by using an equation from Roskam as shown in equation 3.3

For initial cruise sizing consideration, we assumed a value for C_{D_0} for our cruise speed range between Mach 3 to 6 as stipulated in the RFP. By assuming a value for these Mach numbers, and using a drag equation (see Chapter-5), the $(\frac{T}{W})$ required was evaluated by using an equation from Roskam as shown in equation 3.3

$$(3.3) \quad (\frac{T}{W})_{required} = \frac{C_{D_0} q}{\frac{W}{S}} + \frac{\frac{W}{S}}{k q} \qquad q = \frac{\gamma}{2} P_\infty M_\infty^2 \qquad k = \frac{1}{AR \pi e}$$

where k is the same value used in equation 3.1 and q is the dynamic pressure at the cruise speeds M = 3~6. By using these equations, a sizing plot was initially calculated and plotted for all the HSCT planforms. The individual tailoring of the sizing plot was later performed to correct the over-estimated weight of the HSCT aircrafts. All four configurations were found to be under the initial weight estimates. This was a result of the detailed weight component analysis.

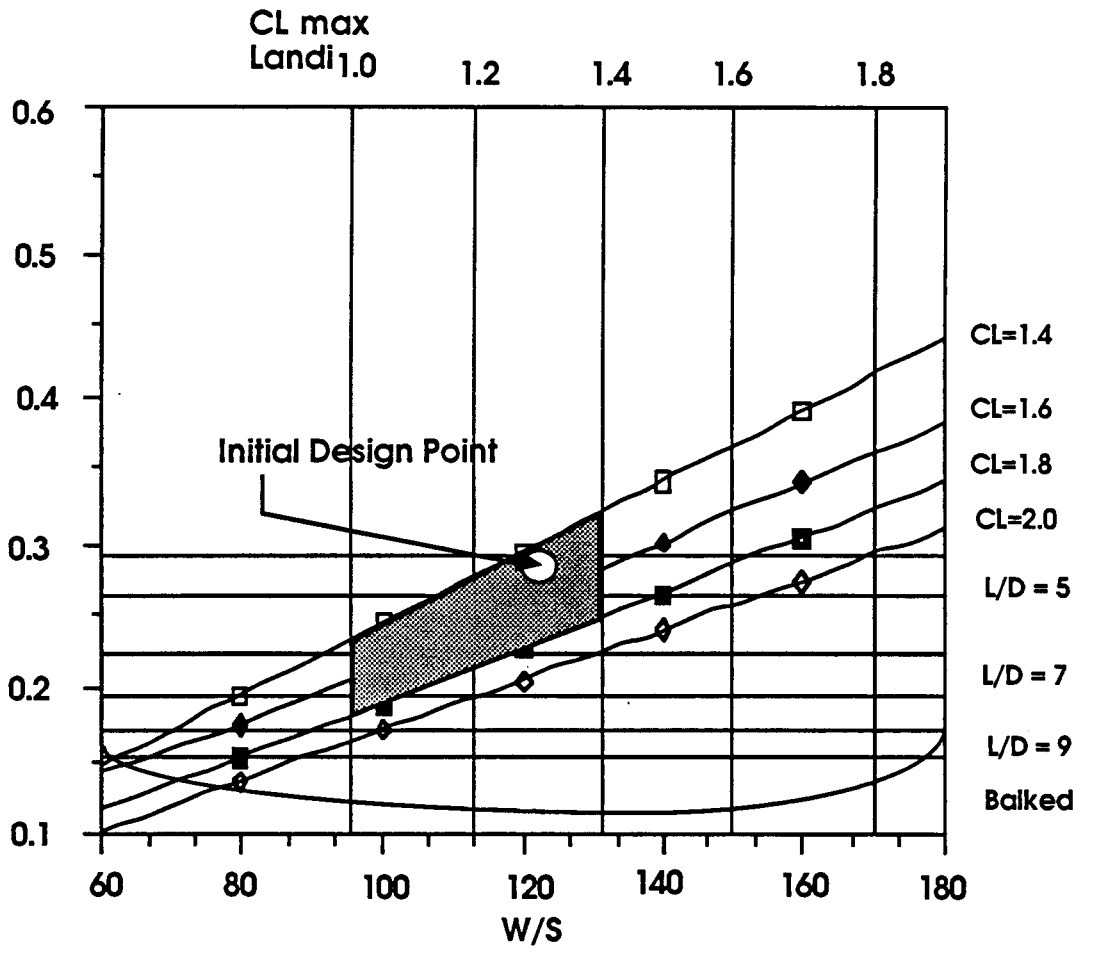

Figure-3.1

3.2 CONFIGURATION SELECTIONS

The final configuration of the Horizon HSCT was determined from a series of prototype configurations that necessitated changes during the evolution stages of this aircraft. The initial designs, consisting two (2) distinctly different configuration as shown in figure-3.2 were put through the initial weight estimate calculations for our mission profile. This process enabled one of the original configurations (BWB-1) to be eliminated to focus concentrated efforts on the development of the remaining aircraft (BWB-2). The next refinements were based on the component weights as well as the cabin, crew and cargo requirements. This process generated our BWB-3 configuration as shown in figure-3.3 to be evaluated for stability and

much needed accurate volume requirement analysis for our mission profile. The next refinements were based on component weights, cabin, crew, and cargo requirements. This process also required our BWB-3 configuration to be evaluated for stability and required an accurate volume determination for our mission profile. Immediately, the BWB-3 was found to lack volume for fuel and was also statically unstable at this configuration. These two problems prompted renaming our BWB-3 with the letter "A" following the designation to acknowledge the modified BWB-3 as reconfigured BWB-3B. The BWB-3B featured a 20 foot increase in overall length and the moving of the delta planform 20 feet to achieve static stability (see Chapter-10). The evolution of the final and current configuration (BWB-4) named Horizon, shown in figure-3.4 was refined from BWB-3B. The major changes for the final configuration were the movement of the inlet-propulsion system on the aircraft to improve area ruling, elimination of sharp corners, and increased effectiveness of vertical tails.

BWB-1 BWB-2

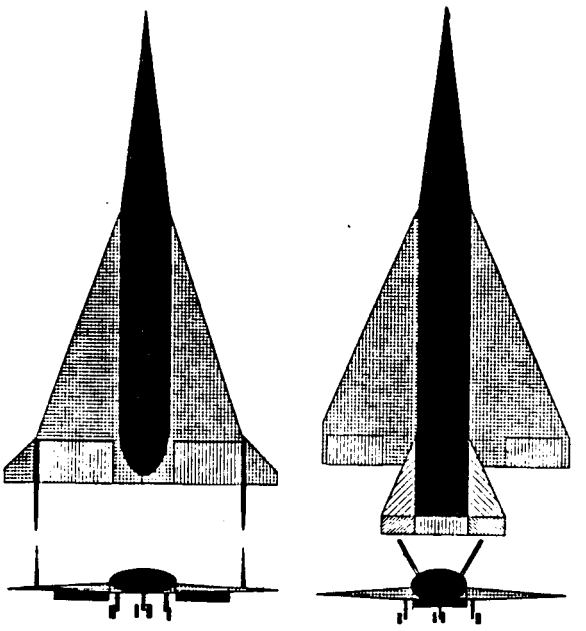

Figure-3.2

BWB-3A BWB-3B

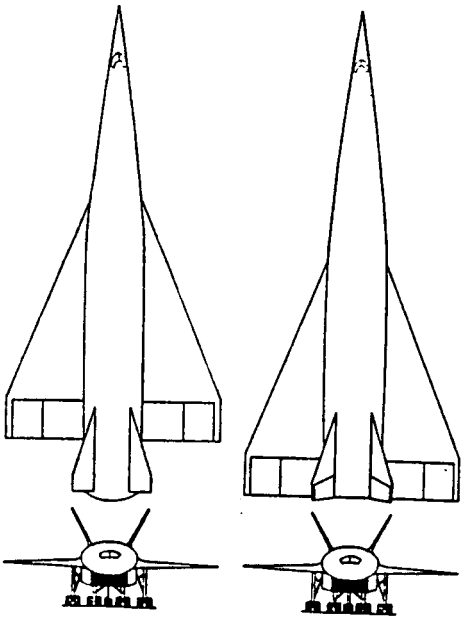

Figure-3.3

Gross Weight : 843,000 lbs
Length : 250 ft
Cruise Mach Number : 5.3
Mission Range : 6,500 nm
Number of Passenger : 222

Wing :
- Area : 8,000 sqft
- Span : 100 ft
- Aspect Ratio : 1.25
- Taper Ratio : .143
- C-bar : 95 ft

Vertical Tail :
- Area ; 1,423 sqft
- Height : 20 ft
- Aspect Ratio : .562
- Taper Ratio : .128
- C-bar : 42.64 ft

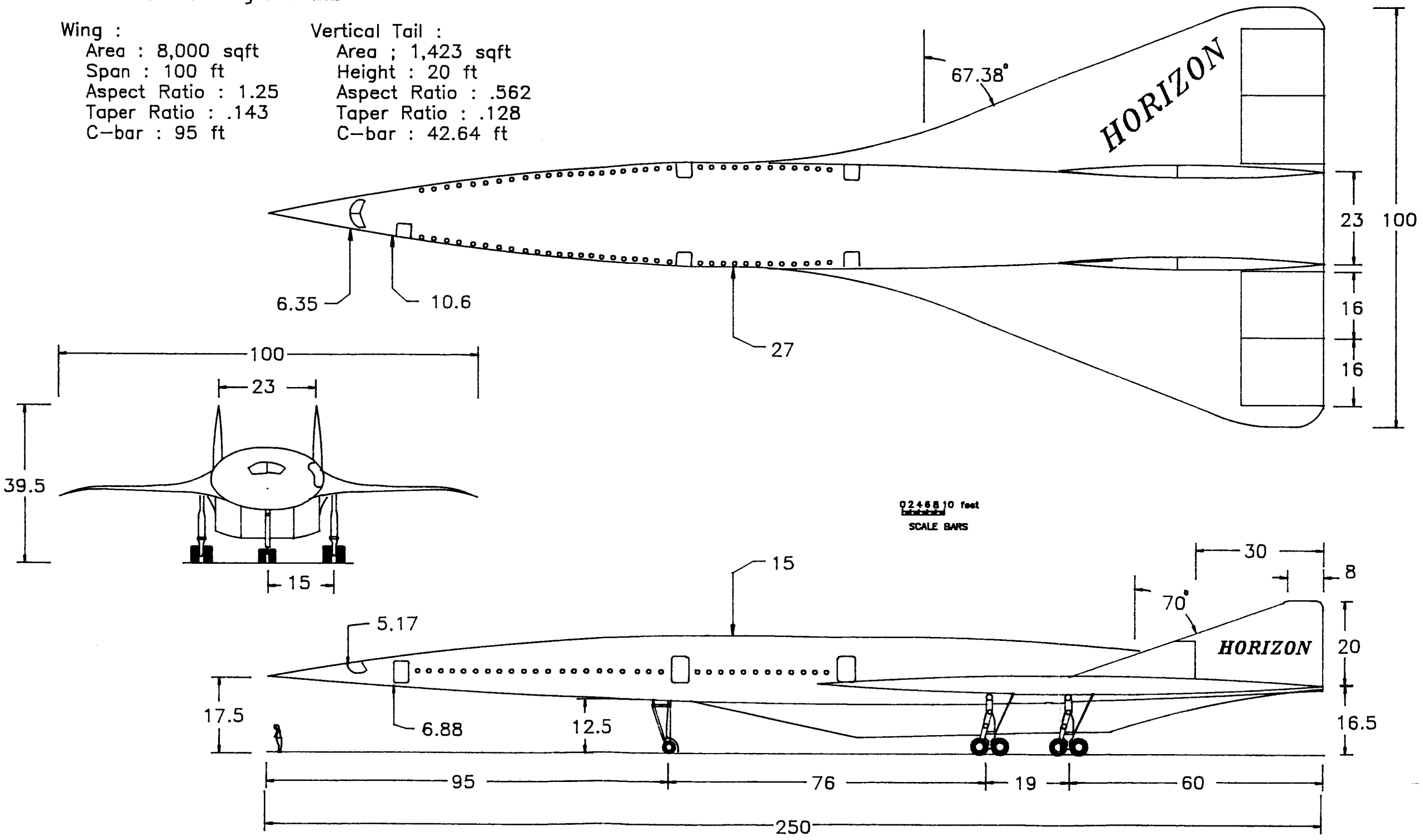

Project Engineer : Paul Keidel
Drawn by Jay Kim

Figure 3.4: Final Configuration

Table-3.1: Summary of Component Weights

wing	77000.0 Lbs
fuselage	200184.8
vertical tail	12088.1
nose gear	3619.9
main gear	14479.6
cowl & duct	10809.8
fuel cell sppts.	3589.5
c.g. control sys.	673.1
engine controls	256.7
engine starting sys.	331.4
surface control hydraulics	8989.0
flight instruments	84.9
engine instruments	39.8
misc. instruments	128.6
electrical sys.	3127.3
flight deck seats	220.0
passenger seats	7110.7
lavatory/water provs.	5148.9
food provs.	2411.4
oxygen sys.	326.2
cabin windows	571.2
baggage & cargo provs.	824.1
furnishings & equipment	660.9
air cond. & de-ice	6187.8
engines	34000.0
fixed weight	50000.0
fuselage fuel, fwd.	180000.0
fuselage fuel, aft	90000.0
wing fuel, fwd.	50000.0
wing fuel, aft	80000.0
gross take-off weight	842863.6 Lbs

3.2.1 PRELIMINARY WEIGHT BREAKDOWN

By considering the take-off weight is made up of the fuel, fixed and empty weights, a weight fraction can be made for any given mission profile. By breaking

down our mission profile into several different phases, the following weight fuel fraction can be made,

$$(3.4)\quad \frac{W_{final}}{W_{take\text{-}off}} = \left(\frac{W_{climb1}}{W_{take\text{-}off}}\right)\left(\frac{W_{climb2}}{W_{climb1}}\right)\left(\frac{W_{cruise}}{W_{climb2}}\right)\left(\frac{W_{descend}}{W_{cruise}}\right)\left(\frac{W_{final}}{W_{descend}}\right)$$

as shown here. The FAR-25 requires that the fuel reserve must be at least 5 percent of the total fuel weight. This amount can be calculated after initial weight analysis. The required fuel amount for loiter time of 30 minutes was also calculated by using this method. The complete analysis of each phase of the weight fuel fraction can be found by using Nicolai's text [Reference-2].

3.2.2 REFINED WEIGHT ESTIMATES

The refined weight estimates calculated from initial weight estimates of the take-off and landing weights. The components used and its corresponding weight values are shown on Table-3.1. The detailed analysis of this method is also given in Nicolai's text [Reference-2].

3.2.3 CONFIGURATION REFINEMENTS

For this section, please refer to the aerodynamics chapter (see Chapter-5) under the effects on general configuration.

3.2.4 SELECTION OF VARIOUS COMPONENTS

Each of the aircraft components were selected under different criteria. Please refer to individual component sections (ie, landing gears, vertical tail sizing, etc.,).

3.2.5 COMPARISON WITH ACSYNT

The NASA/USRA program also included using the NASA developed aircraft synthesis code (**ACSYNT**) to evaluate the design of the aircraft [Reference-3]. The initial dimensions of the configurations BWB-1 and BWB-2 were placed in a format input files on VAX/vms 750 computer where ACSYNT resides, to obtain relative comparison and weight estimates. From these values, the evolutions of subsequent designs were directed and once again employed ACSYNT for further evaluations. The code provided some insights to what an actual design tool was like and also provided the chance to use the code to optimize some of the parameters.

4.0 INTERIOR LAYOUT

4.1 PASSENGER COMPARTMENT

The passenger compartment size was based on default values given by ACSYNT transport passenger section. The values used are 18 inches for each of the aisle width, seat pitch is 38 inches and seat width is 20 to complete the entire passenger compartment as the First Class Section.

The initial study of the HSCT by Boeing and McDonnell Douglas showed the required airfair for airline profitability to be in the neiborhood of $1700.00 for transpacific flight. Based on this information, it was decided that the entire passenger compartment would be designated as a First Class Section. The likelihood of any *"Super Saver Fair"* for this type of aircraft was not foreseen.

The passenger compartment consists of 8 lavatories, 3 galleys and based on the location of the aircraft, the seating ranges from 4 abreast with one aisle to 8 abreast with two aisles. The standard arrangement of 4 abreast in the first class seating is non-applicable in Horizon as Horizon is a wide body aircraft consisting elliptically shaped cross-sectional (dimension of 27 feet wide by 15 feet high at the maximum section) area.

Effort was made to ensure that no fuel was carried either surrounding or under any passenger compartment. The cargo/luggage will be stored underneath the passenger floor which is also pressurized to 8000 feet (FAR-25) altitude to ensure

the safety of the passengers as well as their belongings. The interior layout of the passenger compartment is shown in figure-4.1

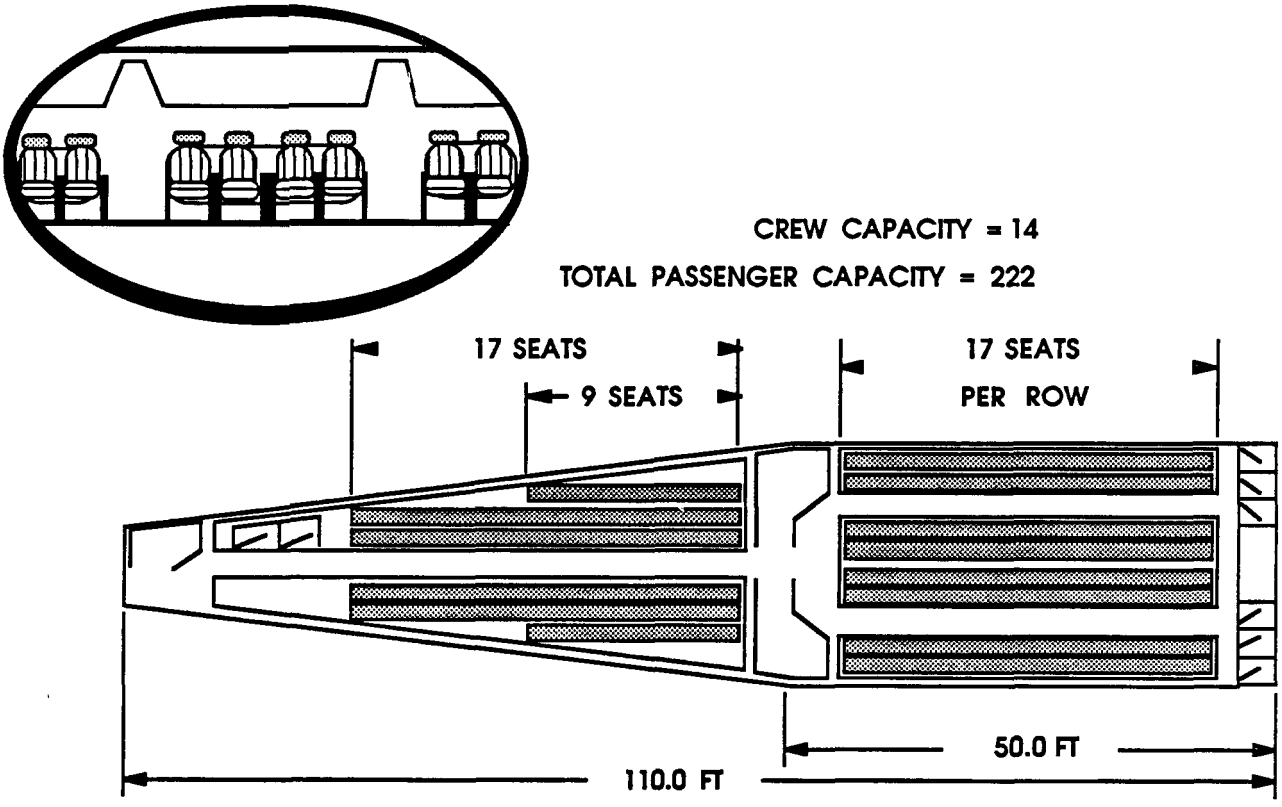

Figure-4.1

4.2 CREW COMPARTMENT

The crew compartment was base on space available in the forward section of the ogive nosed aircraft. The required hardware for this compartment consisted of the control panel with digital CRT and Heads-Up display on the windshield of the aircraft. Two on-board computers controls sensor readings along with commanding the entire Fly-By-Wire control system.

The occupants of the crew compartment consist of the pilot, co-pilot, navigator and mission specialist/systems monitor. To ensure good visibility for the pilot and co-pilot, in addition to ±15 degrees view from horizon, a video output to a CRT is accommodated. The crew compartment is shown in figure-4.2.

5.0 AERODYNAMICS

5.1 INITIAL DESIGN CONSIDERATION

The aerodynamic requirement were initially taken from the sizing chart that was developed. From the sizing chart and required wing loading ($\frac{W}{S}$), the required planform area was identified. For this NASA/USRA study, the group was divided into four distinct planforms. For the blended wing body, total of 8000 ft^2 were necessary to provided an adequate wing loading versus thrust required ($\frac{T}{W}$) design point. Based on this information, the following procedure was used to select the initial design.

5.1.1 SELECTION OF AIRFOIL AND SHAPE OF BODY

One of the critical consideration in selecting the thickness ratio ($\frac{t}{c}$) of the wing section was to minimize the wave drag as much as possible. Yet this wing also has to be practical, meaning thick enough, to manufacture. The thickness ratio or the fineness ratio f=($\frac{c}{t}$) must be at least 3% or f=33.33 to make the manufacturing possible and the thickness limit of this thickness or fineness ratio is to be no more than 6% or f=16.67 to keep the wave drag as low as possible. In the case of most aircraft, especially in case of the commercial subsonic jets, the entire fuel load is carried in the wing. In the case of HSCT, the large fuel requirement from its speed and range, along with thin wing section making this design approach to carry all the fuel in the wing section too impractical to consider (also the need for fuel-c.g. management in subsonic-supersonic transitions). For cooling needs due to aerodynamic heating (see Aerodynamic Heating in this chapter) and the need to relocate the center of gravity (c.g.) during flight, some of the fuel will be housed in

the wing section of the aircraft. The wing section selected for the BWB project is biconvex supersonic airfoil with a sharp leading edge consisting the thickness or fineness ratio of 4% or f=25. The poor low speed characteristics were accepted in favor for the high speed characteristics. The selection of the biconvex (double circular arc) shape over other supersonic airfoil sections *per sa* double wedge or single wedge was due to its increase in available space in the wing section.

The selection of the fuselage shape and its fineness ratio f was based on ideal situation which shows that the minimum C_{D_0} occurs at the fineness ratio f=14. The fuselage fineness ratio is defined as the fuselage length over its diameter $f=(\frac{L}{d})$. The optimum ratio is different for subsonic and supersonic case and the fineness ratio used for this case is that for the supersonic flow. Given this information, the initial design featured the fineness ratio to be $f=(\frac{230}{17})$ or approximately 14. The ogive nose shape was chosen based on its maximum space availability versus minimum drag characteristics. Although a conical shape is known to be the minimum drag body, because of aerodynamic heating consideration and need maximum space, ogive-cylinder combination was used as a base line case.

Since this project was a blended wing-body concept, efforts was made to utilize the triangular planform and the space that surrounded the delta planform. First, to keep all the surfaces within the Mach cone generated by the stagnation region, instead of using a typical circular ogive (where the semi-vertex angle is uniform and would be relatively large, hence causing larger shock angle), the elliptical section shape was used to meet the required flow field in order to keep the delta planform leading edge and vertical tails in the Mach cone. This was accomplished by using a larger angle on the top and side surfaces while using less of

an angle for under surfaces of the aircraft. The design factor for the under surfaces of the aircraft was to provide external compression to the inlet, thereby reducing the amount of work the inlet ramps would have to provide to the flow field. The dimensions used for this task are: semi-vertex angle $\delta_{v_{top}}$=9 degrees, $\delta_{v_{side}}$=9 degrees and $\delta_{v_{bottom}}$=6 degrees.

5.1.2 OVERALL SHAPE

For BWB-1 and BWB-2, the basic shape was chosen and developed from a delta planform with and without the tip chord. The BWB-1 featured smaller vertical tails on the outer portion of planform while the BWB-2 featured lager but canted vertical tail (V-tail). The fuselage used for both are of same dimensions.

5.1.3 AREA RULING

Since the wave drag interference effects in the transonic and supersonic range are greater than those of in the subsonic region due to the higher local Mach numbers of individual components and the larger perturbations induced from this source, the area rule concept was employed in an attempt to reduce wing-body interaction drag. This method is based on the supersonic slender body theory and is a function of the cross-sectional area distribution. This method was used especially for the propulsion system placement. By using a Sears-Haack distribution as the minimum wave drag configuration at M_∞=1, the BWB-3B configuration was fine-tuned into BWB-4 or the Horizon aircraft. The initial and final cross-sectional area distributions are shown in Figures 5.1a and 5.1b.

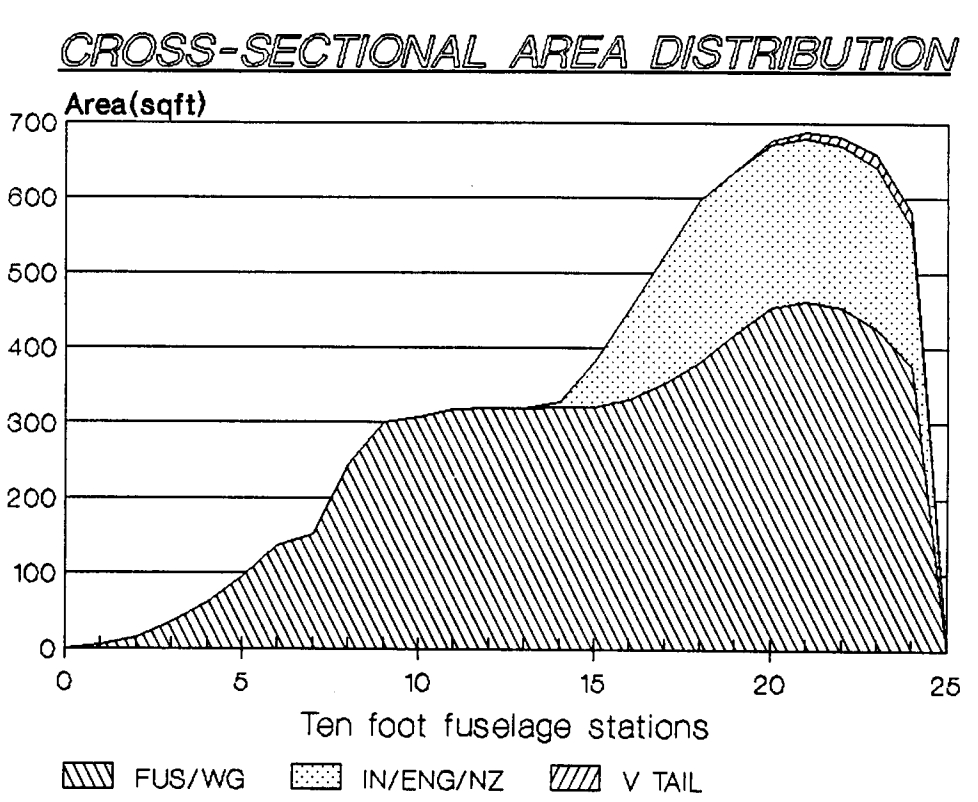

Figure-5.1 a

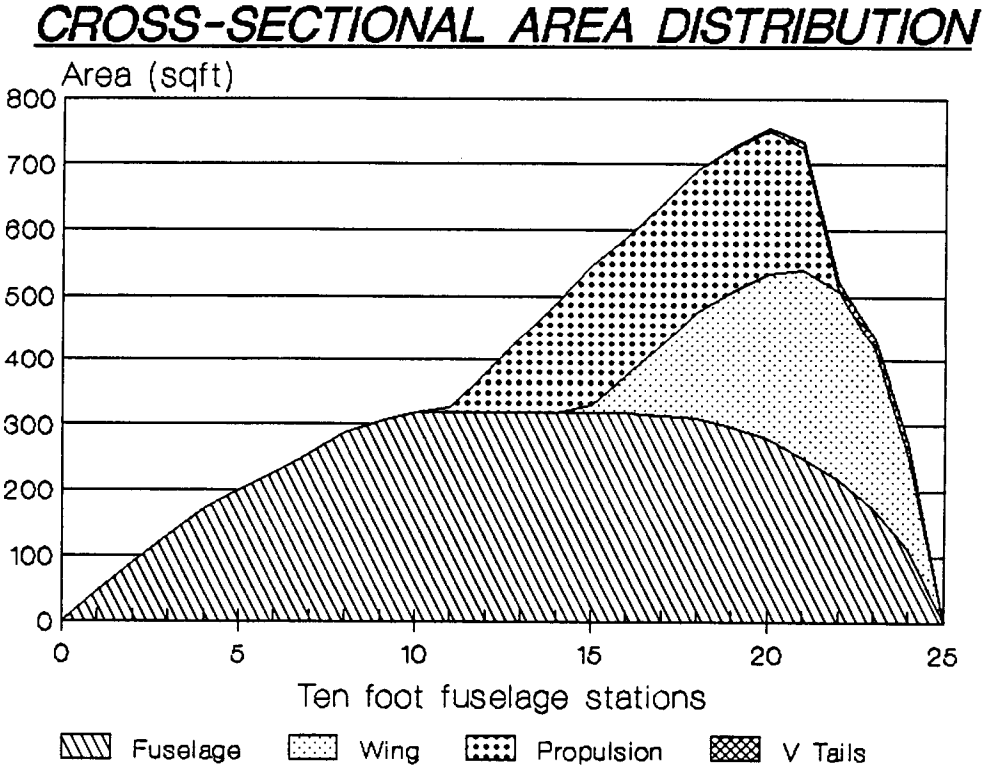

Figure-5.1 b

5.2 AERODYNAMIC CHARCTERISTICS

The following aerodynamic analysis was performed to aid the design goals and evolution of BWB series.

5.2.1 DRAG COEFFICIENTS

To evaluate the drag data, the drag polars as shown in figure-5.2 were constructed using the method of the United Airforce DATCOM [Reference-4]. Each of flight regimes, subsonic, transonic (no exact method) and supersonic was evaluated separately. The method called for the aircraft to be broken down to its components (nose, body, wing, horizontal & vertical surfaces). For complete evaluation the drag components, this must also include the induced drag due to lift. The following basic equations were utilized along with charts provided in DATCOM and Nicolai's text to calculate the drag components.

(5.1) $$C_D = C_{D_o} + kC_L^2$$

(5.2) $$(C_{D_o})_{wb} = (C_{D_o})_{wing} + (C_{D_o})_{body} + \Delta C_{D_o} + C_{D_L}$$

Since most of the drag is due to the the wing, vertical stabilizers and body, the wing-vertical-body combination provides enough information to estimate drag quantities. The actual calculations of these drag values are quiet tedious and is omitted, but one is referred to the DATCOM and Nicolai's text for detailed explanations to obtaining these values. To analyze the initial preliminary design estimates, an easy approximation of C_D, however, was used to check the validity of the design considerations. The equation used for this purpose was taken from Truitt's Hypersonic Aerodynamics text [Reference-5].

$$(5.3)\quad \frac{C_D}{(\frac{t}{c})^3} = \frac{4}{M_\infty (\frac{t}{c})}\{\frac{4}{3} + [\frac{\alpha}{(\frac{t}{c})}]^2\} + \{\frac{(\gamma+1)M_\infty (\frac{t}{c})}{3}\left[[\frac{\alpha}{(\frac{t}{c})}]^4 + 8[\frac{\alpha}{(\frac{t}{c})}]^2 + \frac{16}{5}\right]\}$$

This equation assumes Newtonian Impact Theory.

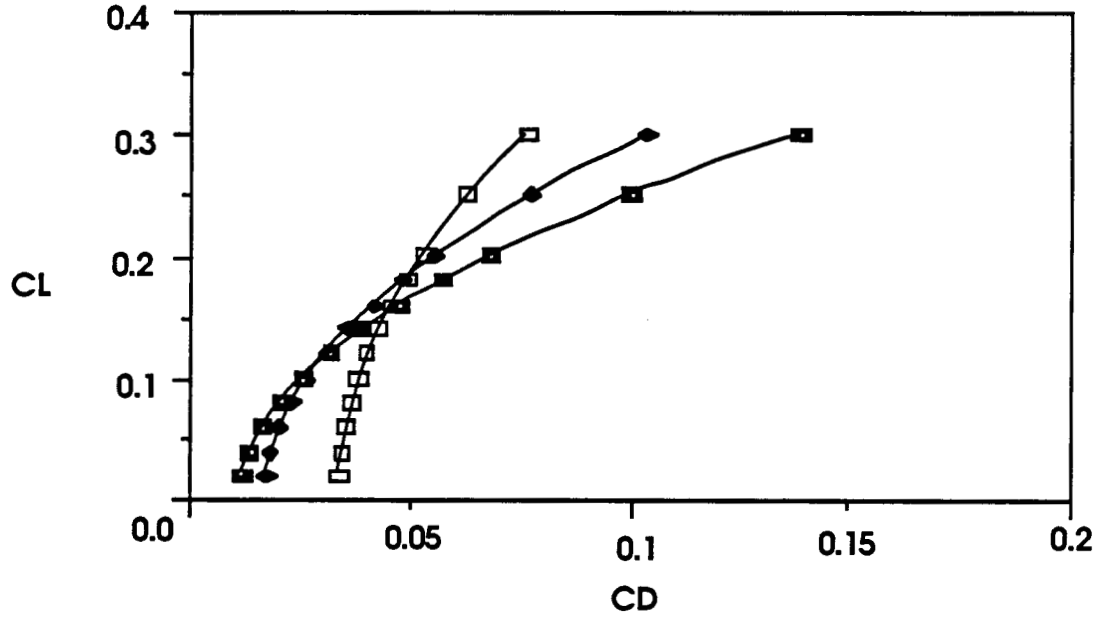

Figure-5.2

5.2.2 LIFT COEFFICIENTS

The basic lift coefficient for the biconvex section was determined by employing the vortex lattice method. The panel method uses a flat plate approximation and this analysis was used with 10 by 4 panels (total of 40 grids) on the delta planform. The $C_{L_{max}}$ was found to be approximately 1, which did not meet the initial sizing requirement. By using the same method, $C_{L_{max}}$ was re-calculated with flap deflections. The required $C_{L_{max}}$ of 1.4+ for the take-off was obtained with

the flap deflection of 30 degrees. The wing lift curve slope is plotted and shown in figure-5.3. The wing stall angle was found to be 33.23 degrees with $C_{L_{max}}$ =1.42.

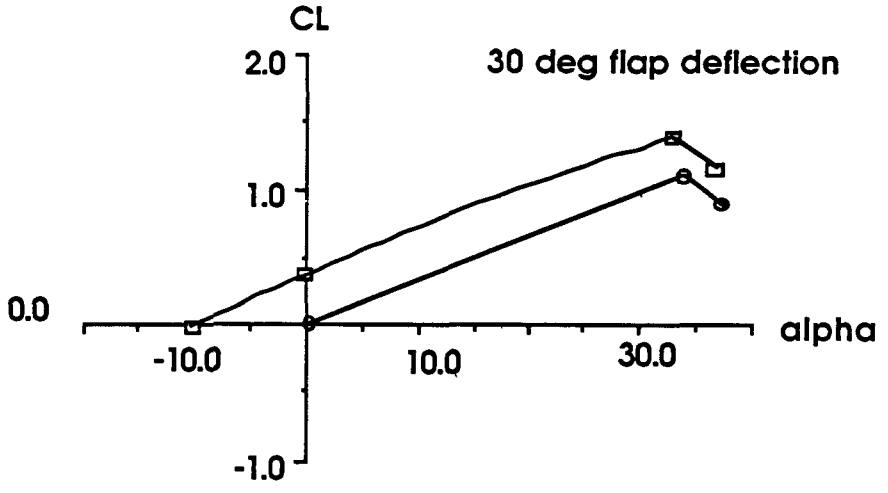

Figure-5.3

To evaluate the preliminary designs, on high supersonic flight characteristics of the wing, the method used once again was taken from Truitt's Hypersonic Aerodynamics text. The following equation 5.4,

$$(5.4)\quad \frac{C_N}{(\frac{t}{c})^2} = 2\frac{\alpha}{(\frac{t}{c})}\{\frac{2}{M_\infty(\frac{t}{c})} + \frac{(\gamma+1)M_\infty(\frac{t}{c})}{6}\left[4+[\frac{\alpha}{(\frac{t}{c})}]^2\right]\}$$

assumes Newtonian Impact Theory.

5.2.3 COMPLETE CONFIGURATION APPROXIMATION

For the body lift, modified Newtonian Impact Theory was used. Though this method is not exact, the purpose of this analysis is to consider the simple component method of determining the aerodynamic characteristics of this aircraft configuration. The primary objective of using these equations are to be used in the

preliminary design purposes and not to complete detailed analysis. For a small angle of attack, the following set of equation can be used to determine the complete configuration lift

$$(5.5)\quad C_D = C_{D_{nose}} \left(\frac{A_{nose}}{S_{wing}}\right) + C_{D_{aftbdy}} \left(\frac{A_{aftbdy}}{S_{wing}}\right) + C_{D_{vt}} \left(\frac{A_{vt}}{S_{wing}}\right) + C_{D_{wing}}$$

$$(5.6)\quad C_L = C_{L_{nose}} \left(\frac{A_{nose}}{S_{wing}}\right) + C_{L_{aftbdy}} \left(\frac{A_{aftbdy}}{S_{wing}}\right) + C_{L_{ht}} \left(\frac{A_{ht}}{S_{wing}}\right) + C_{L_{wing}}$$

DRAG COMPONENTS	LIFT COMPONENTS
$C_{D_{nose}} = C_N \sin(\alpha) + C_D \cos(\alpha)$	$C_{L_{nose}} = C_N \cos(\alpha) - C_D \sin(\alpha)$
$C_{D_{aftbdy}} = \left(\frac{4.8}{\pi}\right) \left(\frac{L_{aftbdy}}{d_{base}}\right) \sin^3(\alpha)$	$C_{L_{aftbdy}} = \left(\frac{4.8}{\pi}\right) \left(\frac{L_{aftbdy}}{d_{base}}\right) \cos(\alpha) \sin^2(\alpha)$

Since the vertical or horizontal tails contributes much less than the nose and the afterbody, it is omitted for this analysis.

5.2.4 MAXIMUM (L/D)

To minimize the fuel use, it is understood that aircrafts should fly about the minimum drag point yielding maximum $\left(\frac{L}{D}\right)$ ratios at the corresponding flight Mach numbers. The determination of the maximum $\left(\frac{L}{D}\right)$ ratio, at a particular Mach number, is discussed in detail in Nicolai's text [Reference-2]. For the BWB aircraft, these values are spotted and shown in figure-5.4, and we were also able to meet the minimum $\left(\frac{L}{D}\right)$ ratio for *one engine out* balked landing FAR 25 requirement. The

Required minimum ($\frac{L}{D}$) ratio was 9.4 for the balked landing and the Horizon with one engine out thrust value can obtain ($\frac{L}{D}$) ratio of 9.81 at just after the take-off condition. Also the maximum ($\frac{L}{D}$) ratios throughout the flight regime were between Truitt's method described above and as indicated in the drag polars, to reinforce the numbers attained were relatively accurate for this analysis.

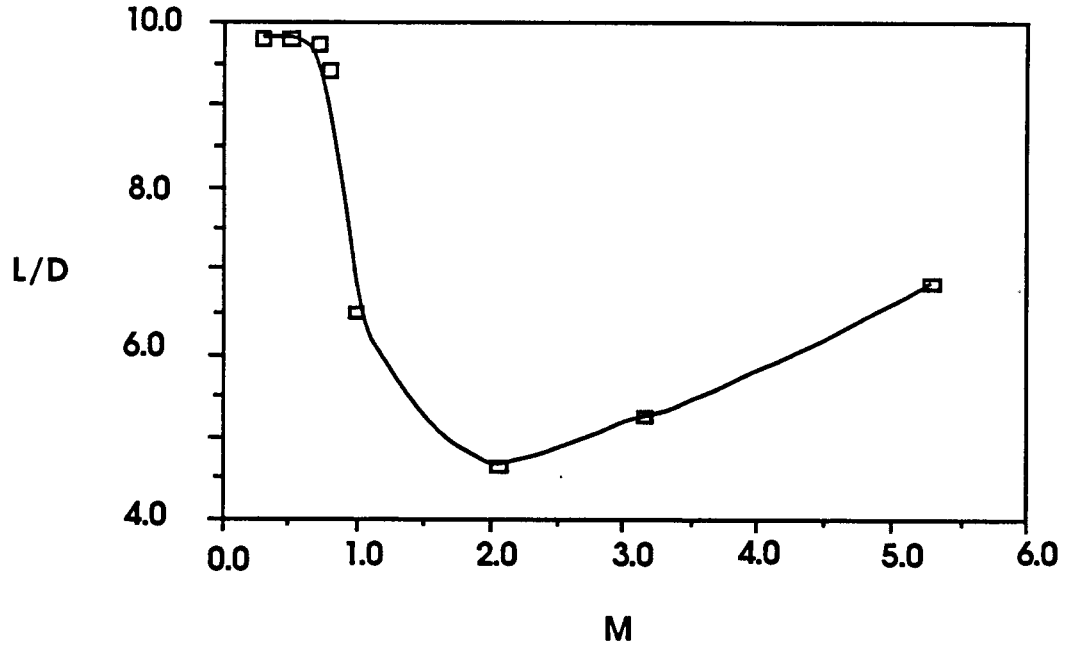

Figure-5.4

5.3 AERODYNAMIC HEATING

Although this is an extremely complicated problem, especially in the turbulent flow, an attempt is made to analyze this problem in a very elementary approach. Since adiabatic wall temperature can exceed the limitation of structural materials commonly used in the aircraft, it is important to consider some of the problems [Reference-6].

5.3.1 ADIABATIC (RECOVERY) WALL TEMPERATURE

It is important to note that in a gases, the adiabatic wall temperature is always less than the free-stream stagnation temperature. From this stated condition, the adiabatic wall temperature can be expressed in terms of Mach number,

$$(5.7)\quad T_{aw} = T_{\infty}\left[1 + R\,(M_{\infty}^{2})\frac{(\gamma - 1)}{2}\right] \qquad R = \text{Recovery factor}$$

$$\text{Laminar} = R = (Pr)^{0.5} \qquad \text{Turbulent} = R = (Pr)^{0.33}$$

where Pr is the Prandtl number ($Pr = \frac{c_p \mu}{k}$)

5.3.2 STAGNATION HEATING

The stagnation region will be heated by a temperature that is close to the total temperature for given Mach number. To evaluate this heat flux, the method used was developed for a re-entry vehicle by Kemp and Riddell [Reference-7].

$$(5.8)\quad q = \frac{17600}{\sqrt{R}}\sqrt{\frac{\rho}{\rho_{SL}}}\left(\frac{U}{U_e}\right)^{3.15}\left[\frac{h_{st} - h_{wall}}{h_{st} - (h_{wall})_{300}}\right]$$

Where q is in ($\frac{BTU}{ft^2\,sec}$), h is enthalpies at stagnation, wall and wall at 300K, R is the nose radius, and U is the free-stream velocity while U_e is the escape velocity of 26000 $\frac{ft}{sec}$. For the BWB, the stagnation nose radius was taken as 0.25 feet and calculated for various Mach numbers and also for our flight conditions. These heat flux are plotted and shown in figure-5.5.

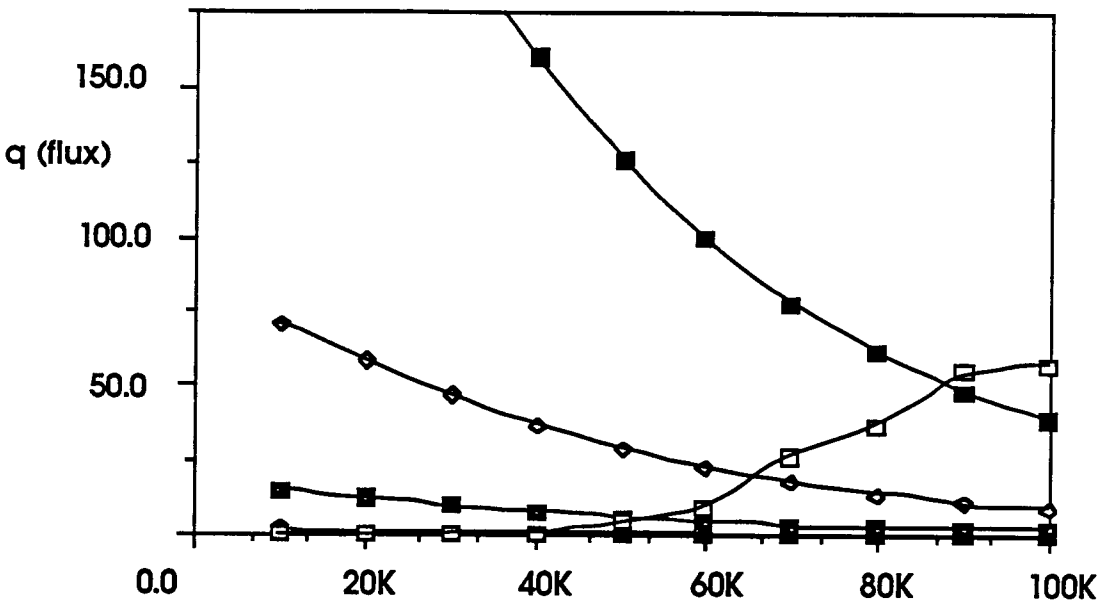

Figure-5.5

5.3.3 EXTERNAL ACTIVE COOLING

Since internal active cooling does not affect external aerodynamics, aside from the cooling the wall temperature to lower the adiabatic wall temperature, the only external active cooling method will be discussed in this section. The method considered was the mass-transfer cooling. There are two (2) type of mass-transfer cooling and they both inject a foreign gas into the boundary layer fluid. If the injection gas is identical with the boundary layer fluid, then the method is known as Transpiration Cooling, while if the injection gas and mainstream fluids are dissimilar, the method is called Mass-Transfer Cooling. The foreign injected fluid can either be liquid or gas fluids. Both type of the mass-transfer cooling method were considered, but due to the additional volume required to contain this extra liquid/gas fluids so that the injection can be made into the boundary layer and considering the HSCT mission profile, it was decided not to use any external active cooling for BWB aircraft. The internal cooling is discussed in the material section of this report.

6.0 Stability and Control

Unless otherwise stated, subsonic and supersonic stability and control flight derivatives were computed using the methods of Reference 1 and Reference 4.

6.1 Subsonic

The planform of Horizon is that of a blended wing-body. Given the initial weight of 1,000,000 pounds and the initial wing loading of 125 pounds per square foot, the sizing chart yielded a wing area of 8000 square feet. In order to avoid tremendous differences in aerodynamic heating of the wing, the wing span was set at 100 feet, so a delta wing planform was chosen for the vehicle. The root chord was 140 feet and the tip chord was 20 feet, the taper ratio was .143, and the airfoil fineness ratio was 25. The leading edge sweep was 67.38° and the trailing edge sweep was zero degrees. This wing was initially 'placed' on the fuselage with 20 feet between the trailing edge and the end of the empanage to allow the possible addition of a horizontal tail.

The referenced methods for computing stability and control derivatives do not account for a (horizontal) tailless vehicle. Values of zero could not be entered for the h-tail surface area and distance to its a.c., so the following assumptions were made. The wing area was kept at 8000 square feet, and the flaperon area was treated as the horizontal tail for the analysis. The a.c. of the h.tail was that of the flaperon, and the span of the h.tail was the same as that of the wing, 100 feet.

In the analysis of static stability and control for the BWB-3A, a positive static margin and pitching moment coefficient was found. In other words, the aircraft

center of gravity(c.g.) was located behind the aircraft aerodynamic center(a.c.) when it was desired to have it in front of the a.c. The first proposed solution was to add a horizontal tail to move the aircraft a.c. back. Horizontal tail sizing produced a horizontal tail which was half as big as the wing. This size was unacceptable structurally. The second proposed solution was to twist and reflex the wing to help move the aircraft a.c. back. The exact determination of twist and reflex would have required an analysis beyond the scope of the initial sizing process.

The final solution chosen was to 'slide' the entire wing back until an acceptable static margin and pitching moment was arrived at. This solution made the most sense because the wing was the largest contributor to the aircraft's a.c. location. With the use of a spreadsheet, all component weights associated with the wing were moved aft in five foot increments, including five and ten feet 'off' the fuselage. Reference 2 suggested that a static margin between five and ten percent of the mean aerodynamic center(m.a.c.) was acceptable for a large transport aircraft. Horizon's static margin fell into this range when the wing's trailing edge was flush with the end of the empanage. The BWB-3B configuration in Figure-3.3 shows the new wing placement. Horizon differs in that all corners have been rounded to decrease the number of aerodynamic heating problem areas(see Figure-6.1).

Vertical tail sizing was the next process to begin. Vertical tail volume coefficients were first taken from the largest transports and yielded a tail size of about 1300 aquare feet. This number was looked at with skepticism for two reasons. First, a single v.tail this size would more than likely extend outside of the cruise Mach cone above the fuselage. Twin tails were immediately decided upon to maintain the area and decrease the heigth. The second reason was that the vertical tail volume coefficients came from subsonic transports, not nearly as fast as the

hypersonic Horizon. Additional comparison data was needed, so the B-58 and B-70 were looked into.

These aircraft were chosen because they were both Mach 2+ delta-winged bombers (see References 14and 15). The B-70 even flew beyond Mach 3. From the data available, the vertical tail volume coefficients calculated were less than five percent larger than those coefficients of the subsonic transports used earlier. Then by extrapolating from the B-58 and B-70 up to the speed of the Horizon, a tail size of just under 1500 square feet was arrived at, a fifteen percent increase from the first estimate. Speed was seen to have a large effect on the size of the vertical tail. (Incidently, data on the Concorde and the Boeing SST was unavailable for comparison).

Dimensions of Horizon used for calculations are listed in Table-6.1. The subsonic static stability and control derivatives were calculated for landing approach speed of Mach .289 at sea level and are listed in Table-6.2. C_{l_β} is more negative than expected, due to the large sweep angle of the wing's leading edge. The shift range of the center of gravity at subsonic speeds is shown in Figure-6.2, based on a full passenger load and five percent of the total fuel load remaining at the end of the flight.

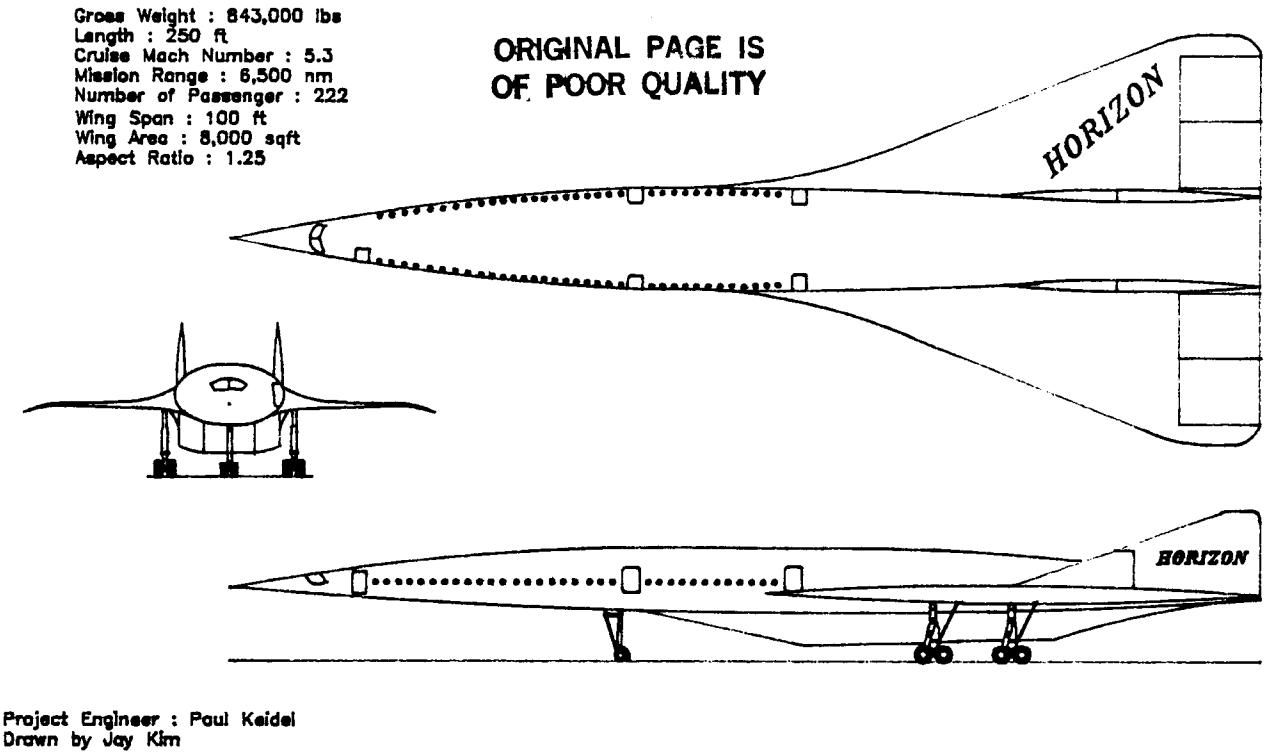

Figure 6.1: Horizon Configuration

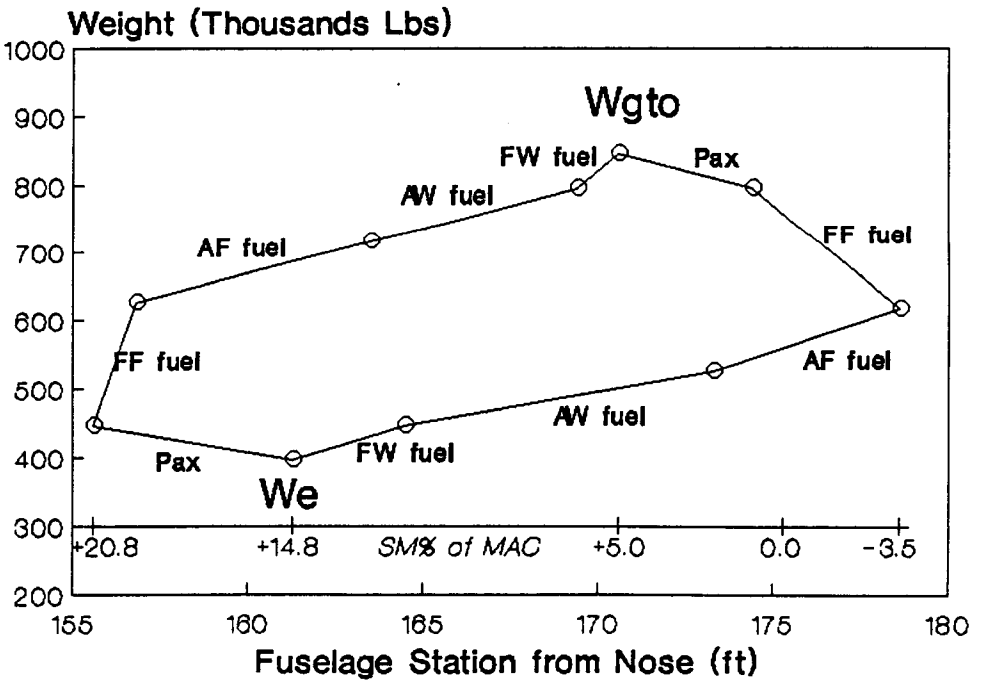

Figure 6.2: Subsonic Center of Gravity Travel

Table 6.1: Aircraft dimensions for input to stability and control calculations

weight	843000 Lbs
avg. fuselage diameter	17.25 ft
dist. btw. $^1/_4mac_w$ & $^1/_4mac_{vt}$	75.60 ft

wing span	100.00 ft	vertical height	20.00ft
wing area	8000 ft^2	vertical tail area	1423.00ft^2
wing aspect ratio	1.25	vertical tail aspect ratio	.562
wing taper ratio	.143	vertical tail taper ratio	.128
wing leading edge sweep	63.78°	v.tail leading edge sweep	70.00°
wing quarter chord sweep	60.94°	v.tail quarter chord sweep	64.11°
wing mid chord sweep	50.19°	v.tail mid chord sweep	53.95°
wing c-bar	95.00 ft	v.tail c-bar	42.64 ft

Table 6.2: Static Stability Derivatives for M=.289 @ sea level

Longitudinal (rad^{-1})

$C_{D_\alpha} = +1.4817$	$C_{D_u} = +0.0000$
$C_{L_\alpha} = +1.6460$	$C_{L_u} = +0.1289$
$C_{M_\alpha} = -0.0410$	$C_{M_u} = +0.0340$
$C_{L_q} = +1.6000$	$C_{M_q} = -0.1730$
$C_{L_{\delta E}} = +0.0000$	$C_{M_{\delta E}} = +0.0000$
$C_{L_{\alpha DOT}} = +1.0090$	$C_{M_{\alpha DOT}} = +0.0000$

Lateral (rad^{-1})

$C_{y_p} = -0.0713$	$C_{y_\beta} = -0.1600$
$C_{l_p} = -0.1129$	$C_{l_\beta} = -0.5710$
$C_{n_p} = -0.1448$	$C_{n_\beta} = +0.1063$
$C_{y_r} = +0.2219$	$C_{y_{\delta A}} = +0.0000$
$C_{l_r} = +0.2526$	$C_{l_{\delta A}} = +0.0588$
$C_{n_r} = -0.1133$	$C_{n_{\delta A}} = +0.0033$
$C_{y_{\delta R}} = +0.3096$	$C_{l_{\delta R}} = +0.0279$
$C_{n_{\delta R}} = -0.0867$	

6.2 Supersonic

Reference 4 states that the supersonic stability and control flight derivatives can be estimated by using the subsonic methods and making sure to change the Mach number where necessary. This method was used, and the supersonic derivatives were calculated for a Mach 1.5 cruise at 45,000 feet and are listed in Table-6.3. There are more values of zero here than in the list of subsonic derivatives, because for some(supersonic), a method does not exist to estimate it and there are no experimental values to compare them to.

Table 6.3: Static Stability Derivatives for M=1.5 @ 45000 ft

Longitudinal (rad^{-1})

$C_{D_\alpha} = +0.4328$	$C_{D_u} = +0.0000$
$C_{L_\alpha} = +3.5780$	$C_{L_u} = +0.0173$
$C_{M_\alpha} = -1.7890$	$C_{M_u} = +0.0000$
$C_{L_q} = +0.0000$	$C_{M_q} = +0.0000$
$C_{L_{\delta E}} = +0.0000$	$C_{M_{\delta E}} = +0.0000$
$CL_{\alpha_{DOT}} = +0.0000$	$CM_{\alpha_{DOT}} = +0.0000$

Lateral (rad^{-1})

$C_{y_p} = -0.0713$	$C_{y_\beta} = -0.4093$
$C_{l_p} = -0.0976$	$C_{l_\beta} = -0.1052$
$C_{n_p} = -0.0083$	$C_{n_\beta} = +0.1063$
$C_{y_r} = +0.2219$	$C_{y_{\delta A}} = +0.0000$
$C_{l_r} = -0.0977$	$C_{l_{\delta A}} = +0.0000$
$C_{n_r} = -0.0642$	$C_{n_{\delta A}} = +0.0004$
$C_{y_{\delta R}} = +0.3096$	$C_{l_{\delta R}} = +0.0279$
$C_{n_{\delta R}} = -0.0867$	

7.0 Propulsion

7.1 Introduction

To date, one of the biggest obstacles in the developement of a high supersonic cruise vehicle is the constraint placed by the technological limitations in the creation of a viable propulsion system. Presently designed vehicles such as the Lockheed SR-71, the Rockwell B-70, and the British Aerospace Concord, have pushed the limitations of technology ever foward. Though the private consumer can purchase passages in relative comfort at speeds exceeding twice the speed of sound, the goal of a vehicle transitting the Pacific Basin in under 4 hours has not been reached. Dubbed the Oriental Express by the general public, the High Speed Civilian Transport (HSCT) requires design performance speeds upwards of 4 times the speeds of sound with an operational range of 6500 to 7000 nautical miles. Such requirements demand the developement of newer and more advanced forms of propulsion to power the vehicle. The two primary forms of engine design that were considered for the HSCT were the Air Turbo-Rocket, referred to as the ATR, and combination engine design of the tubofan and ramjet, referred to as the wraparound.

7.2 Air Tubo-Rocket

Since the early sixties, the air turbo-rocket(ATR) has been examined as a possible altenative and solution to the standard engine designs. The concept of the ATR originated from the promise of increased jet engine performances, gained in the isolation of the turbine from the main engine air flow emmerging from the

compressor and the combustor. The removal of the turbine from the engine flowstream would increase the gross thrust of the engine since a major reduction of the gross thrust was attributed to the driving of the turbine. In `turn, the turrbine would be driven by a suitable rocket motor placed upstream of the turbine, but removed from the main engine flowstream. The ATR is illustrated in Figure-7.1.

Inquiries were made to the private sector on designs and work completed along with some performances of proposed ATR's. Two companies, Aerojet and General Electric, were of prime interests since each has been pursuing the developement of the ATR, independently, for several years. Although the information given by each company were very generous, the resultant datas were deemed unsuitable by the group. As an example, the datas pertaining to the Aerojet engine were only of sea level conditions, having no pertinent information for or conversion for other altitudes. In contrast, the information given by General Electric detailed various altitudes, but, the perfomance provided was insuffiicient. The General Electric datas gave a net thrust of 34,000 lbf. at an altitude of 80,000 ft. with a Total Specific Fuel Consumption (TSFC) greater than 2.0 for Mach number of 5.0.

The eventual solution to the problem was to devise a qualitative analysis for the ATR engine cycle, independently. The procedure utilized to examine rough initial values was to take existing idealized equations for a tubojet engine, assume the turbine will be removed from the incoming engine flow stream, and modify the idealized equation accounting for the assumption. Using the idealized cycle analysis for a tubojet from Reference 1, the resultant equation is,

$$\frac{F}{m_{dot}\, a_0} = M_o \left\{ \sqrt{\frac{\theta_o \tau_c - 1}{\theta_o - 1}\ \theta_b \frac{1}{\theta_o}\frac{1}{\tau_c}} - 1 \right\} \qquad (7.1)$$

Equation 7.1 provided an initial value of gross thrust of approximately 100,000 lbf. for an altitude of 80,000 ft at Mach 5.0. However, a drawback of Equation 7.1 was its lack of incorporating the contribution of the rocket to operate the turbine. A more detailed equation was derived by Ron Mangio to account for the contribution of the rocket in the force equation in addition to another equation for the value of the TSFC.

The values derived for the engine net thrust and TSFC are graphed in Figures 7.2 and 7.3, respectively. From Figure-7.2, the conclusion is that engine was able to provide sufficient thrust at various altitudes and Mach numbers accomodating for the required vehicle operation. For the expected operational cruise altitude of 85,000 ft., the net thrust provided by one engine would be approximately 66,000 lbf. at a freestream Mach number of 5.3, though given the specified net thrust, the TSFC, as shown in Figure 3, would reach 1.4. The conclusion from the TSFC would then indicate the engine performance must be reduced to produce a TSFC to an acceptable level (0.7-.09) in order to make the vehicle economically feasible. The required reduction would demand the engine operate at a lower gross thrust value to conserve fuel. Unfortuanately, with the lowering of the gross thrust, the ram drag remain constant. A reduction in 10% gross thrust may mean a 40% reduction in net thrust. Even with a more favorable gross to net thrust reduction ratio, the amount TSFC must decrease by 30%. This loss may translate to a drop in gross thrust of 40 to

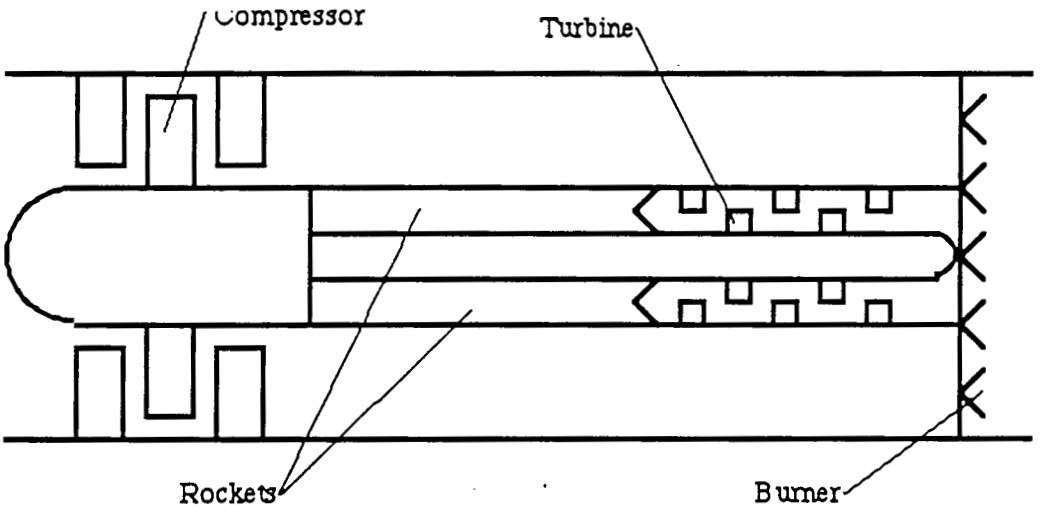

Figure 7.1: Air Turbo-Rocket Engine Schematic

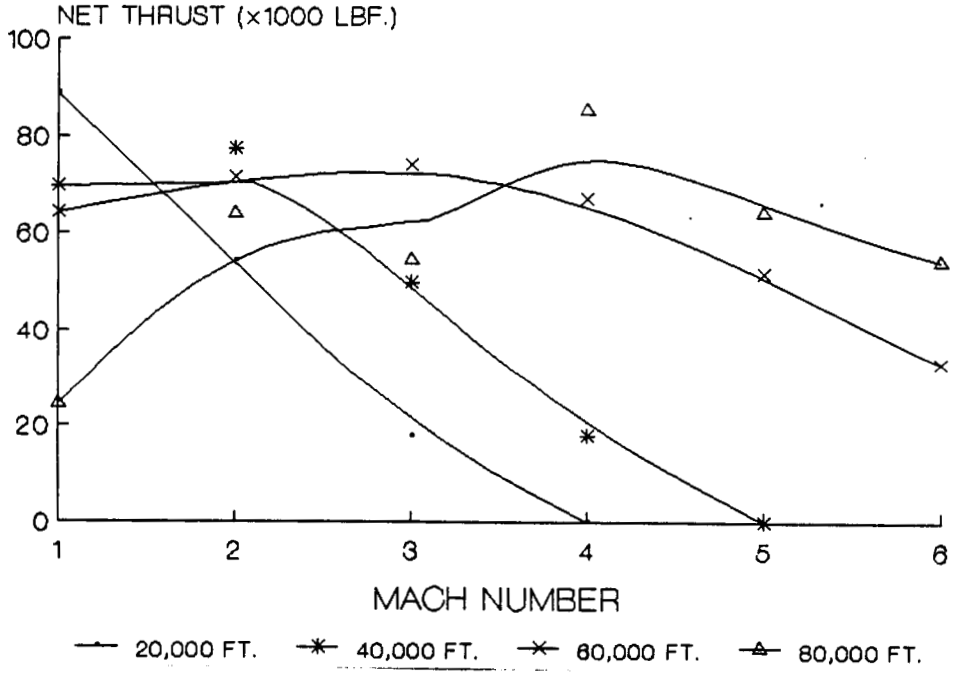

Figure 7.2: ATR Net Thrust vs. Mach Number

50 percent, assuming a relatively linear relation between specific fuel consumption and gross thrust.

7.3 Wraparound (Turbofan/Ramjet)

The second type of engine design considered was the turbofan/ramjet, called the wraparound. A schematic for the engine is provided in Figure-7.4. The wraparound attempts to combined the performance of the turbofan and the ramjet in to a duel engine system. The resultant combination provided the engine with increasd operational versatility superior to turbofan perfomance, with the high Mach number operational capability of the ramjet. As with the ATR, an idealized cycle analysis was developed for the engine system since no adequate source of performance information was attained from researches into past and present programs. From the equations given for the idealized jet engine cycles found in Reference 8, the idealized wraparound performance cycle was developed by combining the turbofan cycle with the ramjet cycle. For the turbofan, the thrust equation is,

$$\frac{F}{m_{dot}a_o(1+\alpha)} = M_o\left\{\sqrt{\frac{\theta_a}{\theta_o\tau_t}\left(\frac{\theta_a\tau_t - 1}{\theta_o - 1}\right)} - 1\right\}, \quad \tau_t = \frac{\theta_t + \theta_o(1+\alpha+\tau_c)}{\frac{\theta_t}{\tau_c} + \theta_o\alpha} \tag{7.2}$$

where the bypass ratio, a, was 3. For the ramjet, the thrust equation is,

$$\frac{F}{m_{dot}a_o} = M_o\left\{\sqrt{\frac{\theta_t}{\theta_o}} - 1\right\} \tag{7.3}$$

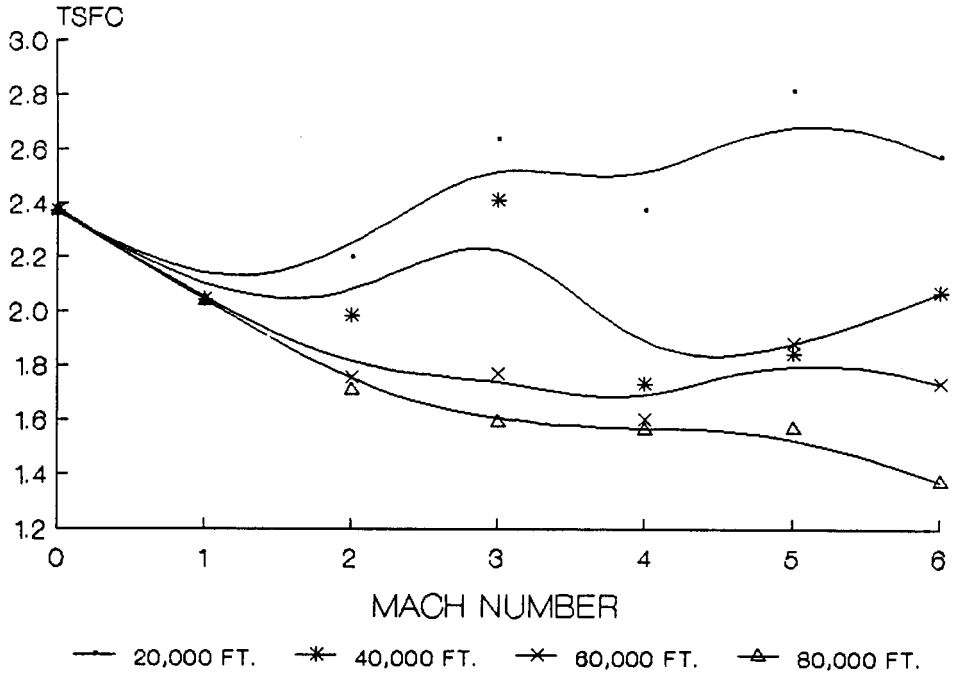

Figure 7.3: ATR TSFC vs. Mach Number

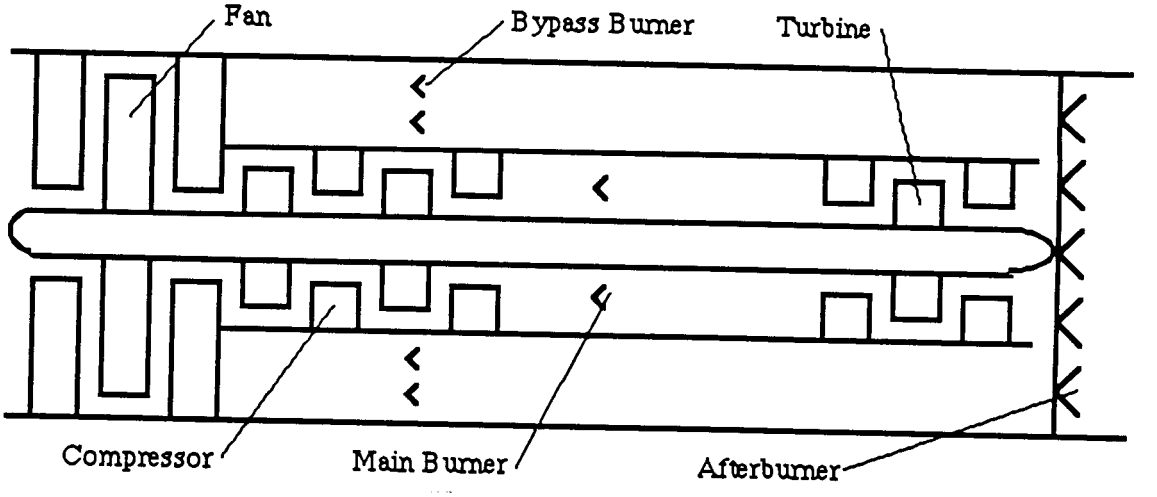

Figure 7.4: Wraparound Engine Schematic

This evaluation assumes the validity of the turbofan cycle with burner in the fan by-pass till a Mach number is reached when the contribution from the compressor and fan are negligable. At the point of minimal contribution, the engine operates as a ramjet. Some engine characteristics were,

Design compressor pressure ratio	14.7(~)
Design turbine temperature	2800°R
Maximum afterburner temperature	6500°R
Maximum ramjet operational temperature	6500°R

The values attained for net thrust and TSFC of the wraparound are graphed in Figures 7.5 and 7.6, respectively. Comparing with the ATR, the wraparound showed a reduced net thrust value. At Mach 5.3, the wraparound provided a net thrust of only 50,000 lbf. in contrast to the ATR output of 66,000 lbf. Examinination of Figure-7.6 would indicate that the wraparound is superior to the ATR in having a dramatically lower TSFC. With a Mach number of 5.3 and an altitude of 85,000 ft., the wraparound provides a TSFC of less 1.0, contrast with the ATR value of 1.4 for the same operational perameter. Hence the reduction in the fuel consumption for the Wraparound would be less dramatical than for the ATR.

Figure-7.7 is a plot of Mach number verses attainable thrust for low altitude operations, assuming idealized turbofan cycle . For the operational range given in Figure-7.7, the TSFC varied between 1.3 to 1.4.

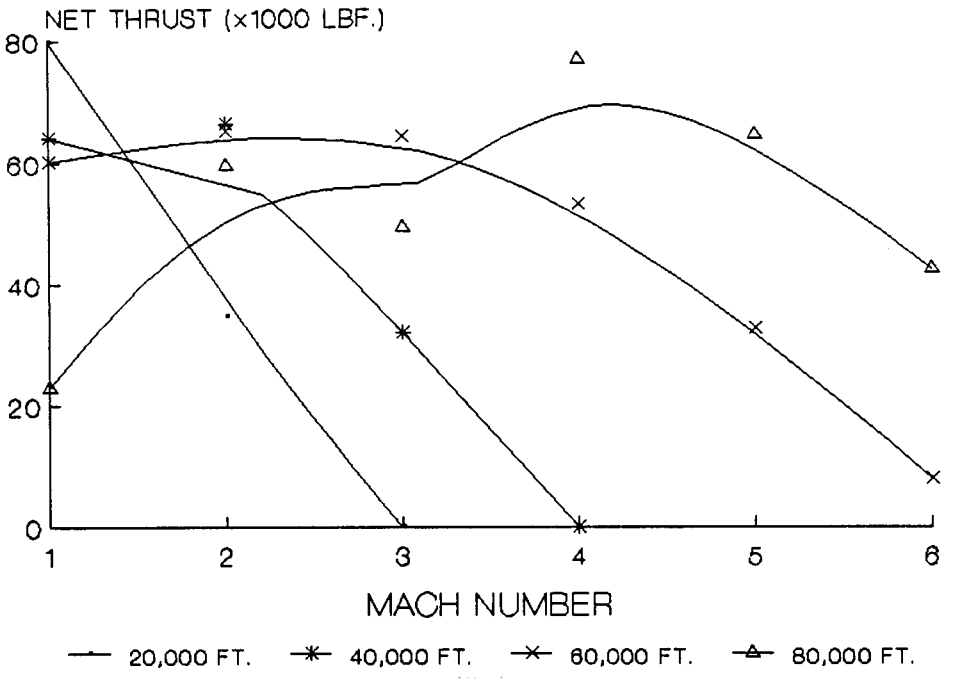

Figure 7.5: Wraparound Net Thrust vs. Mach Number

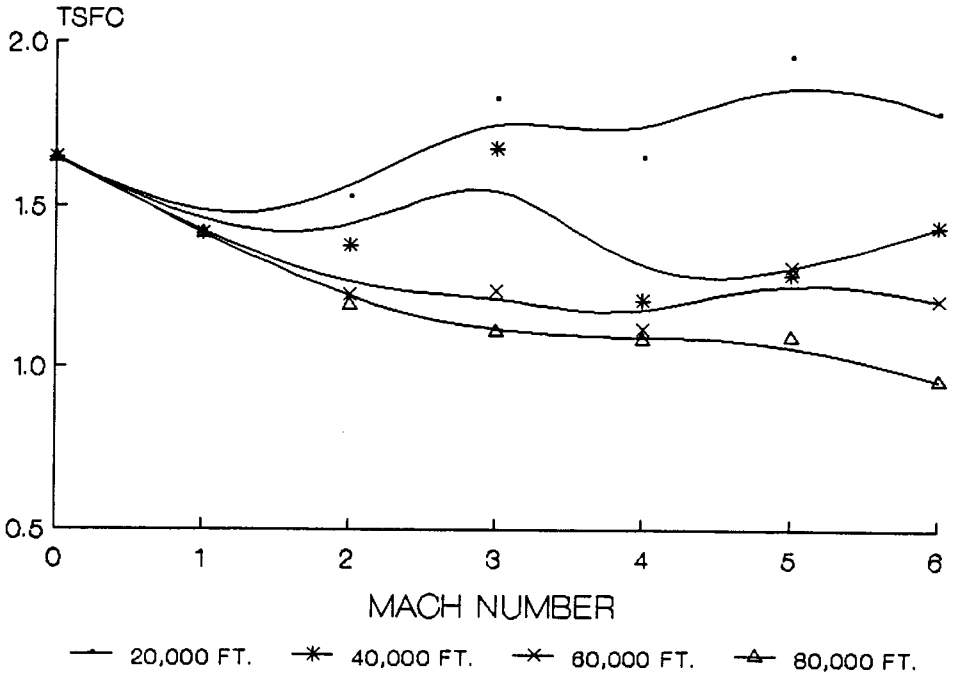

Figure 7.6: Wraparound TSFC vs. Mach Number

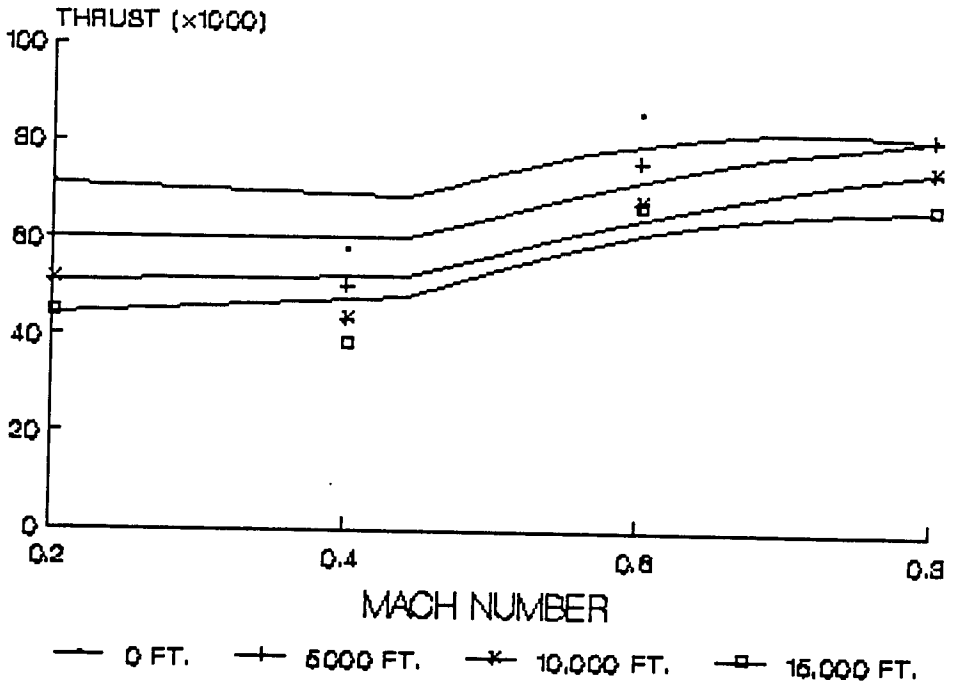

Figure 7.7: Low Altitude Thrust Requirement

7.4 Fuel

An important consideration in the performance of the engine is the type of propellant used by the vehicle. Originally, 3 types of propellants were considered as candidates for the engine: hydrogen, JP-7, and methane. The characteristics of each are compared in Figure-7.8(Reference 9).

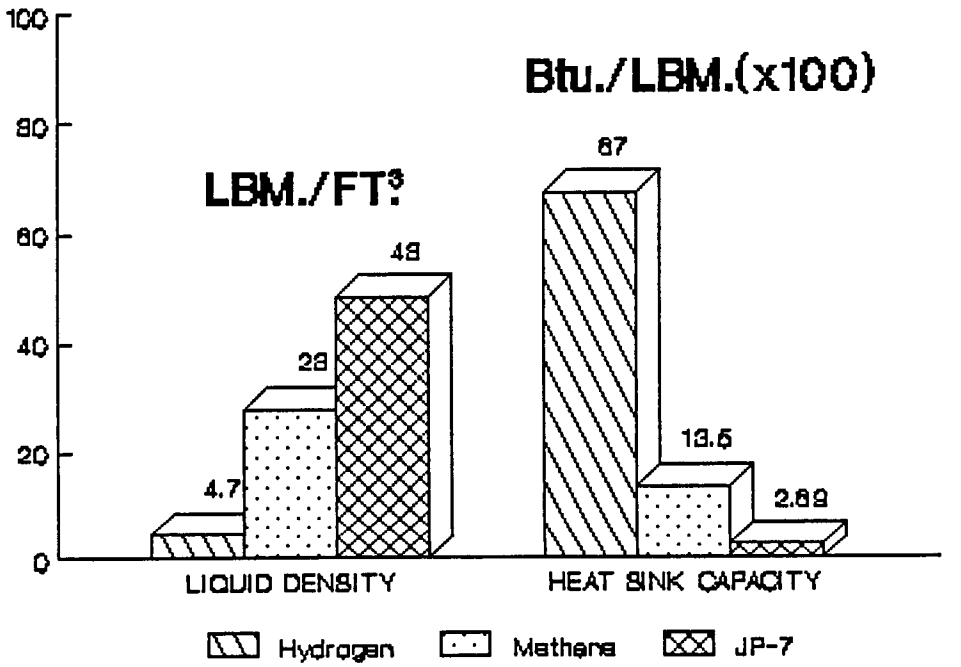

Figure 7.8: HSCT Fuel Comparison

From the given characteristics, the use of hydrogen would increase the complexity of the vehicle since its density is less than 10% of JP-7's given density. The reduction in density will demand a drastic increase in the size of the vehicle in addition to the need of a sturdier and thicker fuel tank wall to maintain the volume

of the hydrogen at an acceptable level. The use of hydrogen may result in an extremely oversided and cumbersome vehicle.

For the case of JP-7, the propellant provides the benifits of being easily handled by the present airport facilities and possessing a very high liquid density. Since portions of the HSCT will be subjected to temperature in excess of 2000°F, the fuel will be used as the prime source of active coolant to avoid carrying additional cooling fluids. Having a heat sink capacity of less than 1/5 of liquid methane and 1/20 of liquid hydrogen, the heat sink capacity of JP-7 may prove insuficient.

The last propellant to be considered was methane. The values showed density of methane is nearly 6 times that of hydrogen, though the heat sink capacity is much lower. Compared with JP-7, the lower density of methane is more than off-set by the increase of heat sink capacity. Thus, methane was deamed the most efficient propellant of the three.

As with hydrogen, methane is also a cryogenic, a quality which may prove objectionable from the stand point of increase support at airport facilities. To counter the objection of increased airport facilities, it should be noted the use of liquid natural gases, such as methane, has existed for some time. The use of liquid natural gas has progressed to a level allowing average consumer the option of purchasing it in large quantities. Any increase in requirements for the storing and usage of liquid natural gas in major airport facilities should not exceed the similar need and cost of accommodating similar increases in JP fuel.

A second problem in the use of methane is bulk storage in the vehicle. Since methane is cooled to a temperature of -260°F, an expected problem of extensive fuel boiloff will result during standard operations of the vehicle. From Reference 10, three primary solution exist for the problem of boiloff; boiloff recovery, subcooling and pressurization, and increase insulation.

The operational regime of the vehicle would cause the liquid methane to be vaperized during flight. The excess vapor may build up to a hazardous level in the fuel tanks, thus requiring a procedure to alleviate the problem prior to the situation becoming critical. One solution would be to vent the excess vapor into the atmosphere, but this may prove impractical since the venting would take place at speeds excesive to the speed of sound. A more practicle solution would be to recover and recycle the fuel vapors back into the engine to auguement the liquid fuel entering the burners. Boiloff recovery may recover as much as 80% of the total vaporized fuel during operations.

A second solution to the presented problem of boiloff would be to futher cool the methane and pressurize the fuel tank. For the methane vehicle given in Reference 3, the use of tank presure at 14.7 psia and a liquid temperature of -268°F provided a 5% increase in the expected passenger capacity . At the lower tank pressure of 6.2 psia, the required subcooled temperature for comparable performance dropped to -284°F, and -293°F for tank pressure of 4.0 psia. If the methane was futher cooled to -298°F, the maximum payload would increase by 15%.

The last proposal was to use insulation around the tank. Again, from the vehicle given, Reference 10 stated that the use of insulation may reduce the maximum payload by less then 3%. An extrapolation to the plane considered in the

project would result in the reduction of less than 7% of the maximum payload (i.e., a reduction of 14 passengers).

Another problem arising from the use of methane would be the accumulation of ice on the wings during ground holds. One solultion to the problem is to use insulation blankets and heat lamps while on the ground. Another solution would require the vehicle to carry nichrome heating wires on the inner suface of the wing skin. Of the two types presented, heating wires would provide the most versatility but may add from 800 to 1000 lbs. to the vehicle weight.

The maximum temperature reached by methane, when burned with oxygen, is to 7000 degrees ^{o}F (Reference 11).

7.5 Inlets

Because of the various required performances of the vehicle, a varible, 2 dimensional, mixed compression inlets were selected for the inlet design. Figure-7.9 shows the proposed design for the inlet at cruise operation. The enlet has a 9.0^{o} fixed initial deflection ramp. At cruise, the second ramp will deflect the ramp an additional 16.0^{o}, given a total of 25^{o} deflection for the first two ramps. The cowl ramp, fixed at 5^{o} from horizontal, deflects the flow back with an additional 5.0^{o}. The supersonic flow terminate at a nomal shock of 1.27. Using Reference 12, the idealized inlet performance behind the nomal shock is,

Static pressure gain	109.4 (~)
Static density gain	27.83 (~)
Static temperature	3.936 (~)
Stagnation pressure recovery	38.4 %

From Reference 13, the diffuser length was calculated with,

$$\text{Tan } q = \{ [(D_{th} - D_{ex})/2] * L \}_d \qquad (4),$$

where $q = 5^o$. The overall inlet dimensions are,

	Length	Width	Height
Inlet	30ft.	7ft.	10ft.
Diffuser	30ft.	7ft.	10ft.

For the captured area, the variable geometry inlet provides the variation in areas needed at the different operating ranges. At take-off, the capture area needed is $30ft^2$. (see Figure 10) to accommadate the mass flow of air. For cruise, the capture area is reduced to $12ft^2$.

To remove the boundary layer, diverters and bleeds were required. As recommended by Reference 13, an initial diverter will be used to remove the boundary layer of the plane's forebody. A secondary bleed was placed at the forward hinge of the second ramp to remove the boundary layer of the fixed ramp. Finally, a shock control bleed will be used to position the normal shock in the throat as well as removed the boundary layer from the second ramp.

7.6 Nozzle

A critical aspect of engine design is the configuration of the nozzle. The nozzel type selected for the vehicle is a convergent - divergent assembly and is shown in Figure-7.10. The nozzel begins with a circular cross-section from the engine, transitioning into a rectangular throat of $17ft.^2$. The nozzle then diverge

into a rectangular exit of area 33ft.^{2}. The selection of a rectangular cross-section for the nozzel was because of the necessity of structural contouring with the aft portion of the aircraft. Since portions of the aft section of the vehicle will be used to assist in the expanding the exit flow, it was thought prudent to avoid the seperation which may result from a circular exit area. The overall length of the nozzle is 24ft. with an efficiency of 0.923. The nozzle is shown integrated with the entire propulsion system in Figure-7.11.

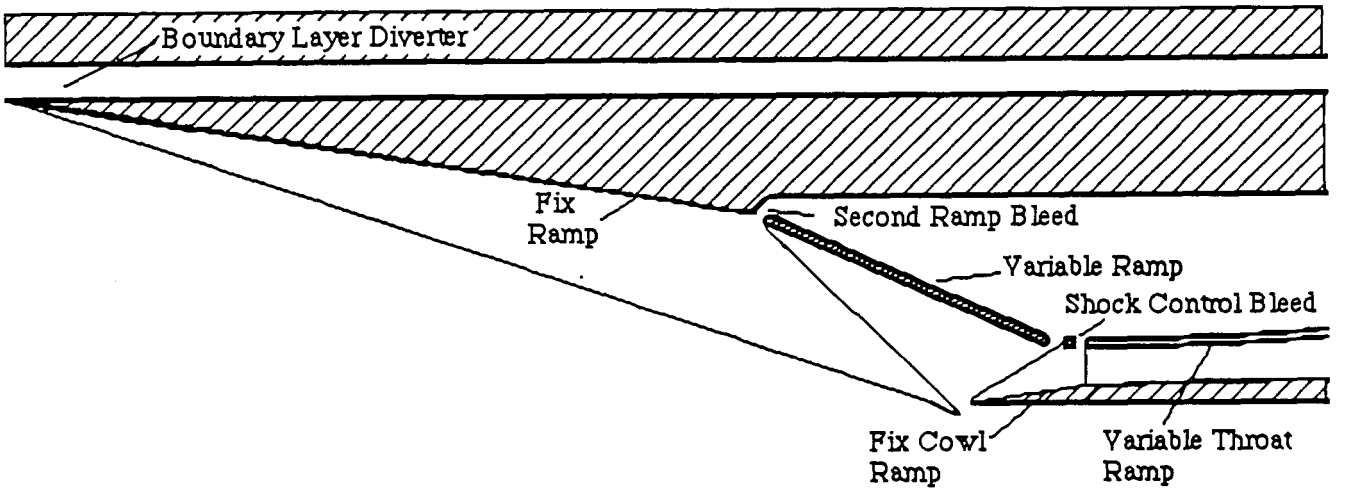

Figure 7.9: Horizon Inlet Diagram

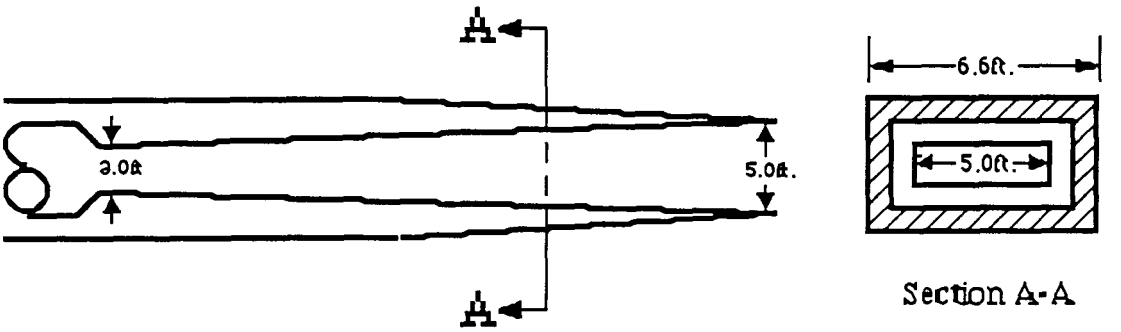

Figure 7.10: Horizon Nozzle Diagram

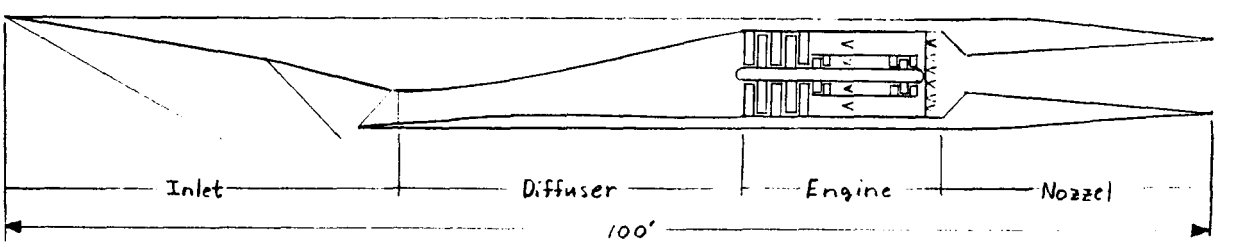

Figure 7.11: Horizon Integrated Propulsion System

8.0 WEIGHTS AND BALANCE

8.1 Weight Breakdown

The Request for Proprosal stipulated a maximum take-off weight of one million pounds. The Horizon has a gross take-off weight of 843000 pounds. The new Boeing 747-400, by comparison, has a gross take-off weight of over 860000 pounds. Hence, the Horizon's weight is typical of today's commercial transport aircraft. The total weight was calculated using methods credited to Mr. H. L. Roland of the General Dynamics Corporation. The weight was broken into five major components including the fuel, wing and tail, propulsion system, fuselage, and interior section(see Figure-8.1). The total weight of the fuel required was determined by summing the weight of the fuel consumed in each segment of the mission profile. The fuel weight of each mission segment was calculated by multiplying the specific impulse, velocity, and the time for that segment. The fuel accounted for 47.2 % of the gross take-off weight. This is to be expected when the range, 6500 nautical miles (nmi), that is covered in a typical mission is considered. Twenty-three percent of the gross take-off weight was due to the fuselage while the combined weight of the wings and tails contributed 12.4%. The propulsion system, which included four engines, engine controls, fuel systems, starting systems, lubrication systems, cowl and duct, and the air induction system, accounted for 5.4% of the weight. The remaining 11.3% of the weight was due to the fuselage interior. This component consisted of the flight controls, provisions, landing gear, and passengers. An allowance of 220 pounds (lbs) was made for each passenger and their carry on baggage.

8.2 Center of Gravity Travel

The center of gravity (c.g.) is the most important element in the stability and control of an aircraft, therfore, its location should not be left to chance. It is suggested in Reference 2 that the static margin (SM) be between +5% and +10% of the mean aerodynamic chord (MAC) for transport aircraft. Larger static margins lead to trim drags that are not tolerable. In order to get a SM of +5 to +10 it was necessary to experiment with the placement of certain components. Figure-6.2 reveals that this goal was accomplished. This was done by moving the wing back 20 feet aft(see Figure-3.3). In addition, the utilization of a fuel sequencing system was proposed. The result of these accommodations can be seen in the c.g. envelope of Figure-6.2. The graph shows that the SM is +5% MAC at take-off. As the Horizon proceeds through its mission fuel is consumed and the location of the c.g. changes. The fuel in the forward wing is used initially. The resulting shift in the c.g. location is small. The SM changes from +5% to +6%. The aft wing fuel is then used. The SM moves toward 12% as the remaining wing fuel is consumed. The fuel in the aft section of the fuselage is then used; the SM moves to 18% as this portion of fuel is burned. Finally, the fuel in the forward section of the fuselage is consumed. At 20.8%, the SM is largest at this point. The last shift in c.g. location comes about when the passengers are unloaded. The SM decreases from 20.8% to 14.8% as the passengers get of the plane. Thus the maximum shift in the c.g. location is approximately 15% of the MAC.

8.3 Fuel Management

As mentioned earlier, the location of the c.g. must not be left to chance. The c.g. location has to be controlled so that the stability and control characteristics of the

vehicle may be maintained throughout an entire mission. The most common way to control c.g. travel is to move the fuel around to various locations on the vehicle during flight. This causes the mass distribution of the aircraft to change, hence the c.g. location changes. The proposed fuel management system is shown in Figure-8.2. The fuel is sequenced in the following manner: aft wing, forward wing, aft fuselage, forward fuselage. The first lengthwise tank is the forward fuselage tank and the last two tanks are the aft fuselage tanks. The wing tanks are divided into eight fuel cells. The triangular cells are the forward tanks while the remaining tanks are combined to form the aft tanks. The fuel management system is also responsible for pumping the fuel to various stations on the leading edges of the wings where the fuel will act as a heat sink to cool the wing surface.

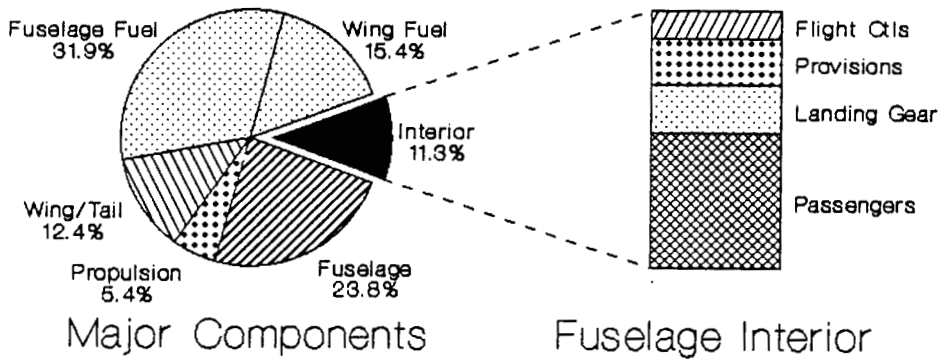

Figure 8.1: Major Component Weight Distribution

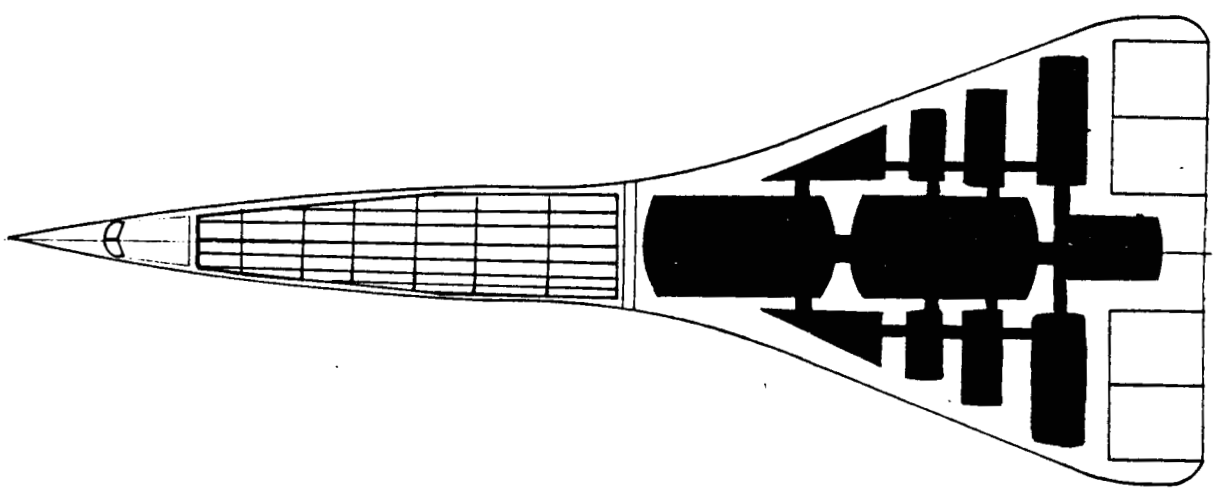

Figure 8.2: Fuel Cell Schematic

9.0 Performance

9.1 Take - off analysis

For analytical purposes the take-off consists of a ground run, rotation and climb over a 50 ft obstacle as required by FAR 25. Therefore, the total take-off distance is the sum of the ground distance, rotation distance, transition distance and climb distance. However, in the case of one-engine-inoperative on take-off, balanced field length(BFL) should be considered as run-away distance. It is the sum of the distance required to accelerate to the critical engine failure speed and the distance of either continuing the take-off over a 50 ft obstacle with one engine inoperative or braking to a full stop. With a take-off weight of 843,000 lbs and a take-off speed 357 ft/sec, take-off distance has been calculated as 9,600 ft and the balanced field length(BFL) was determined to be 11,040 ft at sea level on a standard day. This take-off distance satisfies the RFP which requires a field length of 11,500 ft. Figure-9.1 illustrates the geometry used in the analysis of the take-off . And Figure-9.2 shows variable take-off distance with respect to altitude and temperature variation.

9.1.1 Ground Distance S_G

With the maximum take-off weight of 843,000lbs, a wing area of 8,000 sqft , and the maximum lift coefficient of 1 at sea level, the take-off speed is calulated as

$$V_{TO} = 1.2\, V_{stall} = 1.2 \sqrt{\frac{W}{S} \frac{2}{\rho C_{Lmax}}} = 357 \text{ ft/sec}$$

REQUIREMENTS

1. TAKE-OFF WEIGHT : 843,000 lbs
2. TAKE-OFF SPEED : 350 ft/sec
3. THRUST-to-WEIGHT RATIO AT TAKE-OFF : .28 - .4
4. AERODYNAMIC DRAG AND GROUND FRICTION COEFFICIENT : .11 & .03
5. PILOT TECHNIQUE

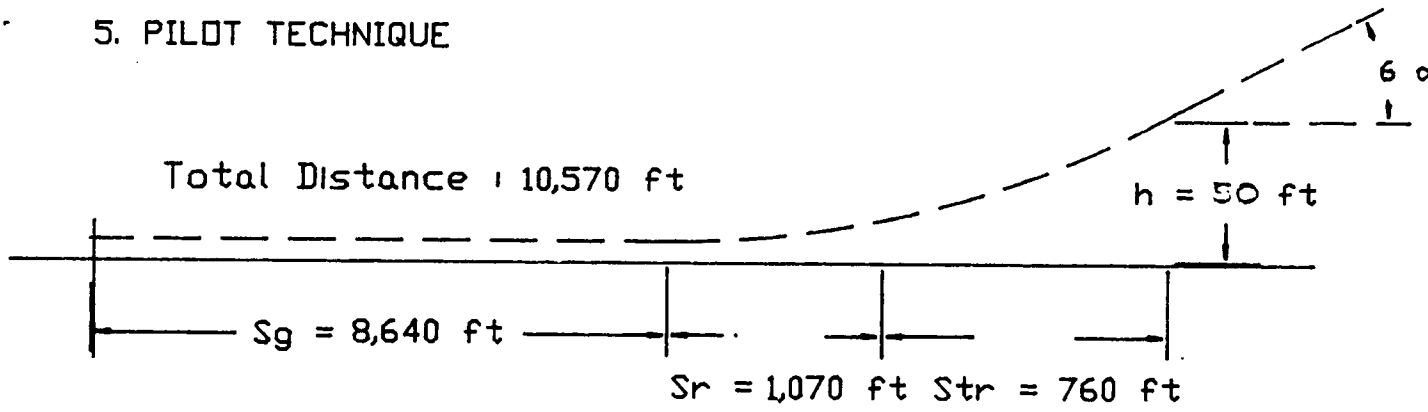

TAKE-OFF TIME : 54 SEC

RATE OF CLIMB : 1640 fpm

BALANCED FIELD LENGTH (BFL) : 11,040 ft

Figure9.1:Take-offDistanceDiagram

For ground run, with a flap angle of 35 deg., the lift coefficient in ground effect and drag are calculated to be .38 and .0285 respectevely. With these values, the net acceleration force at $V_{TO}/1.414$ is determined as

$$F_a = (T - \mu W) - (C_D - \mu C_L)\, qS = 195{,}800 \text{ lb}$$

and the ground distance as

$$S_G = \frac{W}{2g}\frac{V_{TO}^2}{F_a} = 8{,}160 \text{ ft}$$

9.1.2 Rotation Distance S_R

Refer to Reference 2. The rotation takes a fixed time of about 3 sec. and the rotation distance is calculated with angular rotation more than 5 deg. as

$$S_R = t_R V_{TO} = 1{,}070 \text{ ft}$$

The pilot must be careful not to over-rotate the airplane, or the tail will strike the ground during this rotation.

9.1.3 Transition Distance S_{TR}

For maneuvering into this flight segment, the radius of the circular arc flare has been calculated as 8,960 ft. The rate of climb at take-off is given by

$$R.C. = V \sin\theta_{CL} = \frac{V(T - D)}{W}$$

and climb angle has been calculated as 9.21 deg. . The transition distance is determined as

$$S_{TR} = R \sin\theta_{CL} = 1{,}430 \text{ ft}$$

However, for this transition distance, the transition height is greater than 50 ft. By working back to 50 ft., the transition distance is re-calculated as 370 ft.

9.2 Rate of Climb

The rate of climb for a steady climb is given by

$$\frac{dh}{dt} = \frac{Pa-Pr}{W}$$

The turbojet/ramjet engines used by the Horizon produce variable power with respect to altitude and velocity changes up to the crusing altitude. The thrust required for Horizon is shown in Figure-9.3. From these estimated power available and thrust required curves, the rate of climb at different altitudes and Mach numbers have been calculated and plotted in Figure-9.4. Absolute ceiling and service ceiling for the Horizon are also indicated.

9.3 Loiter

For flight at a fixed altitude and Mach number , L/D and specific fuel consumption C are constant with respect to weight so that the expression for the endurance of a jet aircraft is given by

$$E = \frac{L}{D}\frac{1}{C}\ln\frac{W_i}{W_f} \text{ hrs.}$$

It is observed that in order to obtain maximum loiter for a given weight change, the aircraft should fly at an altitude and Mach number such that (L/D)(1/C) is a maximum. To satisfy this requirement, at 40,000 ft and Mach .3, the maximum value of (L/D)(1/C) has been selected as 6. And given the initial take-off weight of

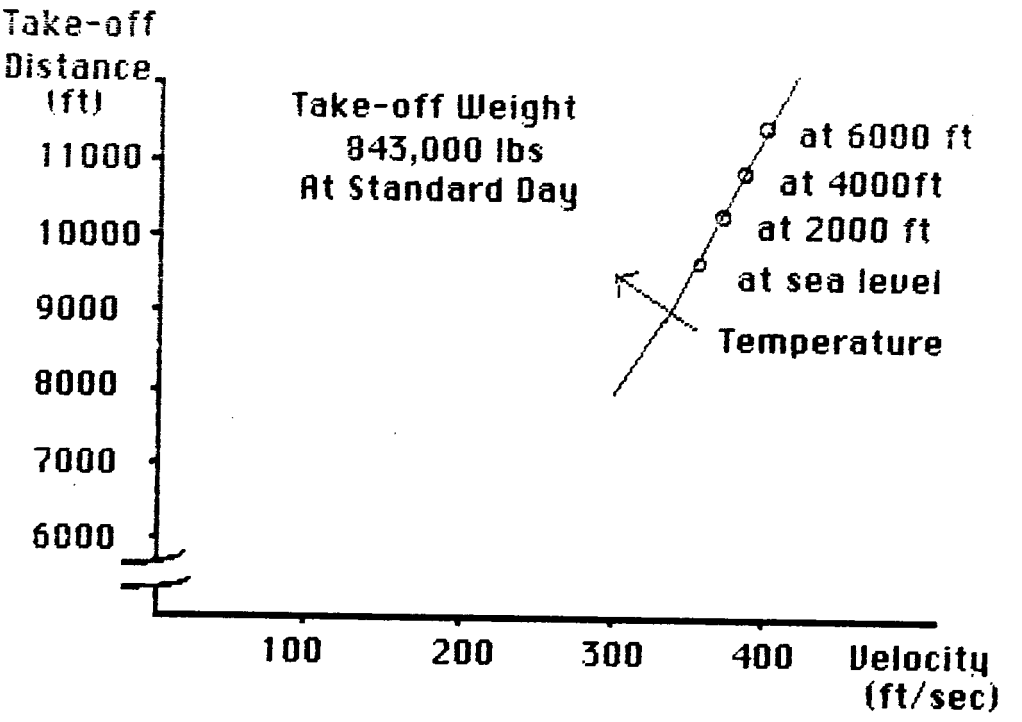

Figure 9.2: Take-off Distance vs. Velocity

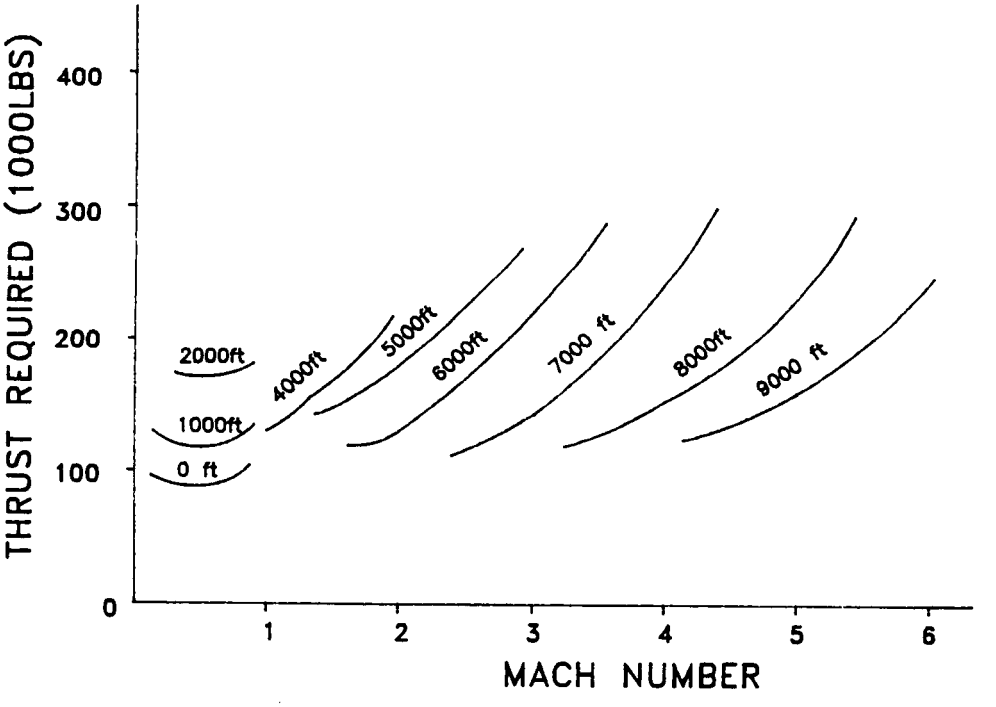

Figure 9.3: Thrust Required vs. Mach NUmber

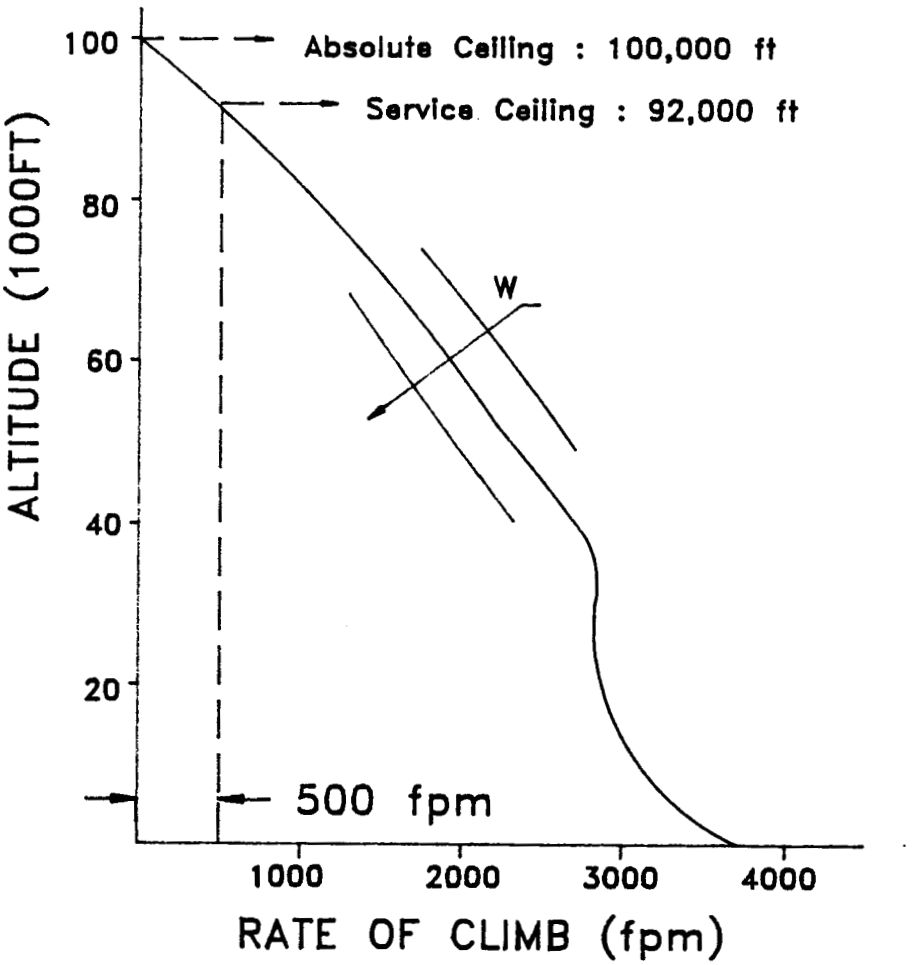

Figure 9.4: Altitude vs. Rate of Climb

843,000 lbs and final cruise weight 650,000 lbs , the lotier time is calculated to be 1 hour and 30 minutes, which is three times the amount required.

9.4 Landing Analysis

The landing performance is similar to the take-off performance varying only in the treatment of the approach and flare and in the consideration of auxiliary stopping devices such as speed brakes. The term 'approach' applies only to the air distance from an altitude of 50 ft to touchdown. After touchdown, there is a short ground run without applying the brakes called a free roll distance and the remaining ground run with full brakes to a complete stop. . With the maximum landing weight of 650,000 pounds and approach speed of 300 feet per second, the landing distance is calculated to be 8,560 ft. Figure-9.5 shows the schematic used for the previous analysis and landing distance at sea level on a standard day.

9.4.1 Air Distance, S_A

It is assumed that the approach speed is equal to the legal minimum, 1.3 V_S, where V_S is the stall speed in the landing configuration. In the flair, the airspeed will be reduced from Mach .3. At touchdown, it is assumed to be $V_{td} = 1.15\ V_S$. At a landing weight of 650000 Lbs, the approach speed and touchdown speed have been calculated as 340 ft/sec and 300 ft/sec respectively. The air distance is found to be

$$S_A = \frac{W}{D}\left[\frac{V_A^2 - V_{td}^2}{2g}\right] = 2488\ \text{ft}$$

REQUIREMENTS

1. LANDING WEIGHT : 650,000 lbs
2. APPROACH SPEED : 340 ft/s
3. DECELERATION METHOD USED : Brake (Coefficient is .4
4. FLYING QUALITIES OF THE AIRPLANE
5. PILOT TECHNIQUE

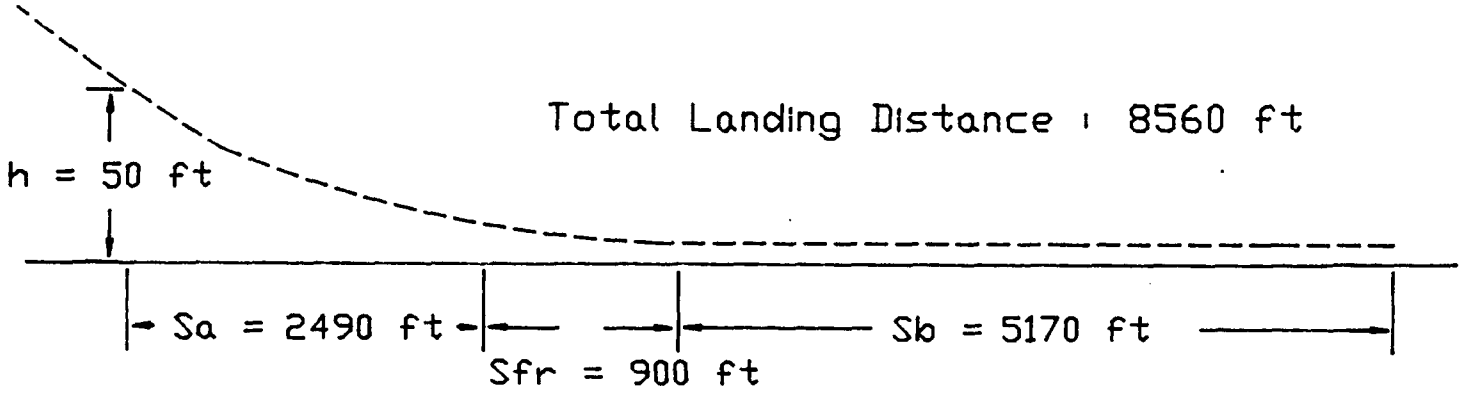

Figure 9.5: Landing Distance Diagram

9.4.2 Free Roll Distance, S_{FR}

Similar to rotation distance is the time for the free roll, t_{FR}, taken as 3 sec. The free roll distance is calculated as

$$S_{FR} = t_{FR} V_{td} = 900 \text{ ft} \quad .$$

9.4.3 Braking Distance

With a static braking force of $F_S = \mu W = 26000$ Lbs. and the braking force at the beginning of brake application $F_B = \mu_B W - (\mu_B C_L - C_D) q S = 11960$ Lbs, the braking distance is calculated as

$$S_B = \frac{W}{2g} \frac{V_{TD}^2}{F_m} = 5170 \text{ ft} \qquad \text{where} \quad F_m = \left[\frac{1 - \frac{F_B}{F_S}}{\ln(\frac{F_S}{F_B})} \right] F_S$$

9.5 Landing gear design

To position the landing gear on the aircraft, the center of gravity range of the aircraft is determined. The c.g. was located on 177 feet back from the nose and the range extended it 25 feet forward. To determine the number and size of the wheels and tires to be used on each strut, the maximun static load per strut was calculated as 50,000 pounds for the nose gear strut with two tires and 200,000 pounds for each main gear strut with four tires each. Using this information and the tire data [Reference 1], the type of tires chosen is shown in Table-9.1.

Initial landing gear placement located one main gear strut on each side of the engines where the wing joined the fuselege. There were six tires per strut, and the

space for landing gear retraction was reduced. However, it was found that more tires per strut did not change the weight 'foot-print' of the aircraft which was beyond 400,000 pounds each---too heavy for existing runways[Reference 1]. So it had been changed to have two main gear struts on each side with four tires each. Landing gear lay-out is shown in Figure-9.6.

Figure-9.6 also shows that the landing gear design satisfies the longitudinal and lateral criteria. There is at most 95% of the vehicle weight on the main gear. For the nose gear, there have been some problems as to where to locate it. Beacause of foreign object damage, locating the nose gear in front of the inlet was not a good selection. However, the nose gear just behind the inlet put it too close to the main gear. So, the nose gear was placed in front of the inlet with a splash guard which will prevent dirt and rocks and water from being thrown into the inlet. The landing gear retraction sequence is shown in Figure-9.7.

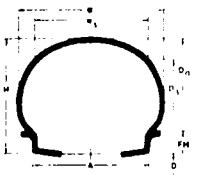

	Tire Discription			Tire dimension(in)						Max Loading (lbs)	Unloaded Inflation Pressure (psi)	Max Speed (MPH)	Weight (lbs)
				Do		W		Ds	Ws				
	Do	W	D	Max	Min	Max	Min	Max	Min				
Nose	40	x 14		39.8	38.9	14	13.3	35.1	12	25,000	155	255	112
main	50	x 20	20	50.0	49.0	20	19.1	44.6	17.6	53,800	190	225	240

Table 9.1: Tire Selection

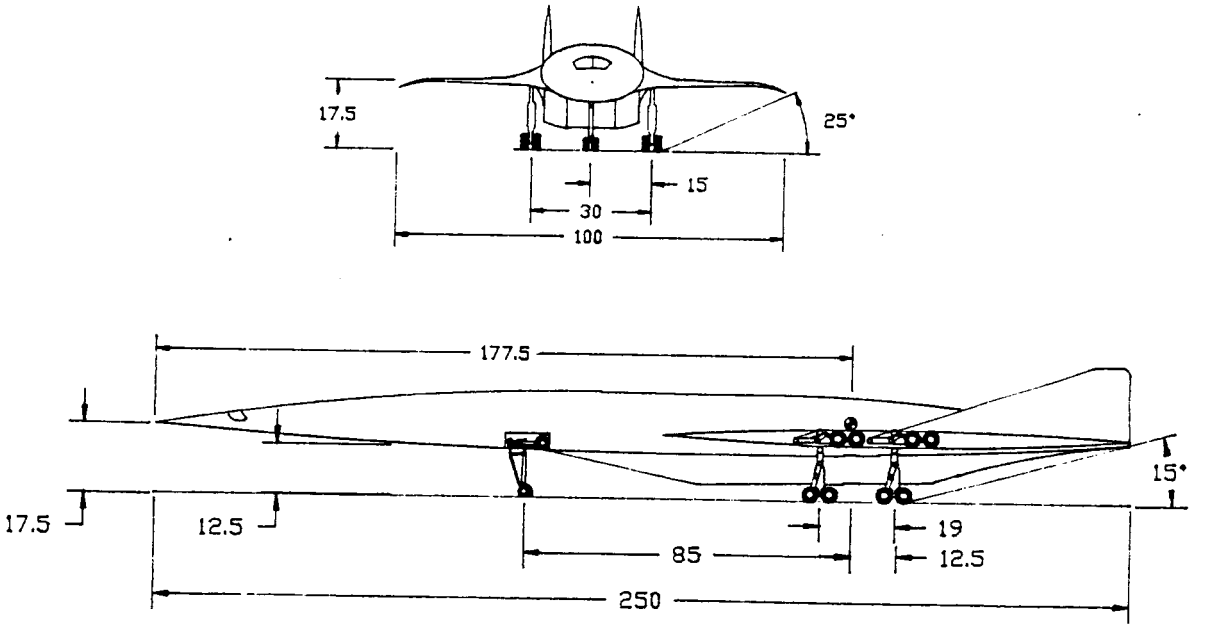

Figure 9.6: Landing Gear Layout

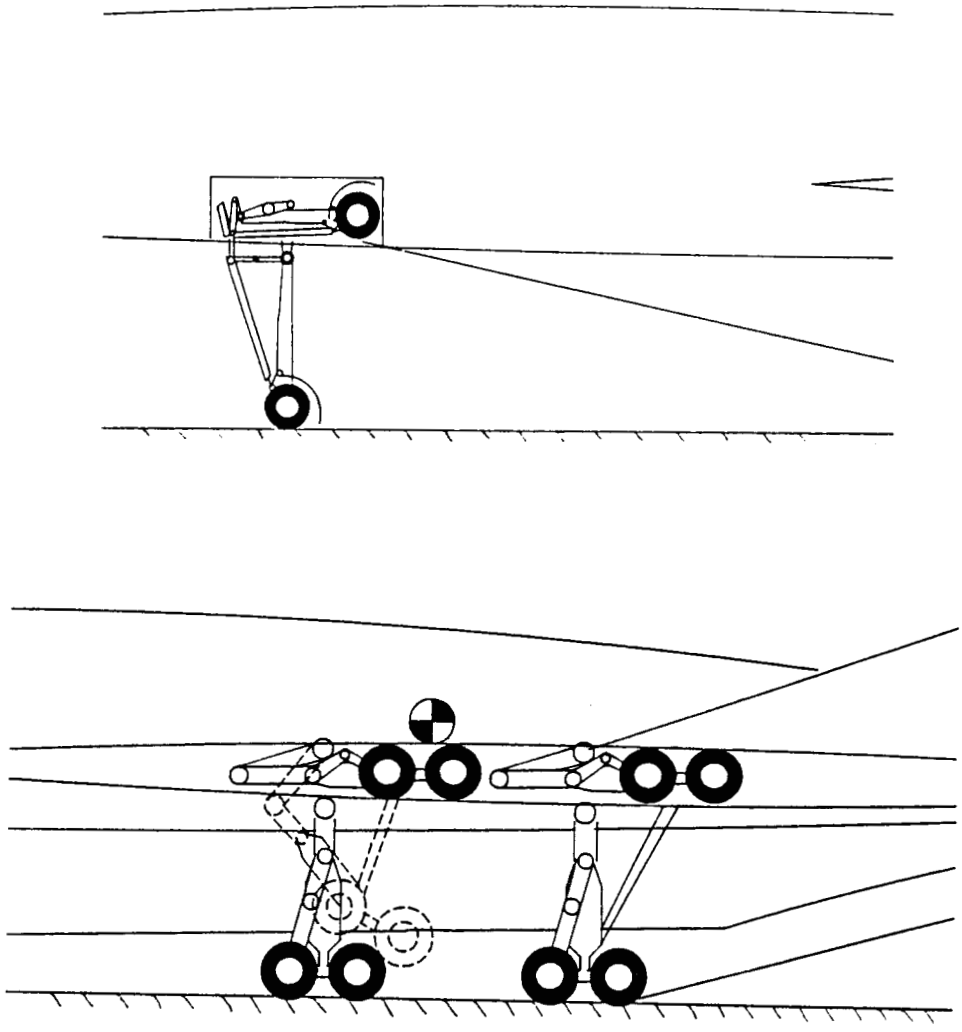

Figure 9.7: Landing Gear Retraction Sequence

10.0 Heat Transfer

10.1 Cooling

Intrinsic to supersonic flight is aerodynamic heating. Section 5.3 discusses the chacteristics and effects of aerodynamic heating upon a plane surface.

A model which simulates the aerodynamic heating on a plane surface was created by Mr. Pablo Martinez of Cal Poly Pomona. This model revealed that surface temperatures of up to 1200 ° Farenheit could be experienced by the stagnation points and leading edges of the vehicle. At these extreme temperatures, cooling techniques had to be considered. Research indicated that the structure could be cooled by using combinations of high temperature insulation, bare structures, and convectively cooled overcoats if needed.

11.0 Structures

11.1 Acceleration Loads

The velocity - load diagram shown in Figure-11.1 was constructed according to the requirements specified in the Federal Aviation Regulation (FAR), part 25. The V-n diagram tells the designer how much structural integrity must integrated ino the design of the vehicle. Based on the calculated gross take-off weight of 845863 lbs, the positive limit load factor was determined to be 1.49. However, FAR 25 also states that the positive limit load factor may never be less than 2.5, therfore, the default value of 2.5 was used. The maximum negative limit load factor was assumed to be -1.0. Using the gross take-off weight and a maximum take-off lift coefficient of 1.6, the stall speed, V_{stall} , was calculated from Equation-11.1 to be 224.78 ft/s (133.18 knots). This is the minimum speed at which the aircraft can maintain steady state flight. The design maneuvering speed, V_A, was determined from Equation-11.2 to be 210 knots. The design speed for maximum gust intensity, V_B, was 146 knots. This speed was determined by the intersection of the V_B gust line and the $C_{N_{Max}}$ line. The design cruising speed, V_C, and the design diving speed, V_D, were 189 knots and 548 knots, respectively. Equations 11.3 and 11.4 were used to calculate these values.

$$V_{stall} = [\, 2(W_{TO}/S) \,/\, r_{SL}\, C_{N_{Max}} \,]^{1/2} \qquad \text{Eq. 11.1}$$

$$V_A = V_{stall}\, n_{lim}^{1/2} \qquad \text{Eq. 11.2}$$

$$V_C = V_B + 43 \text{ knots} \qquad \text{Eq. 11.3}$$

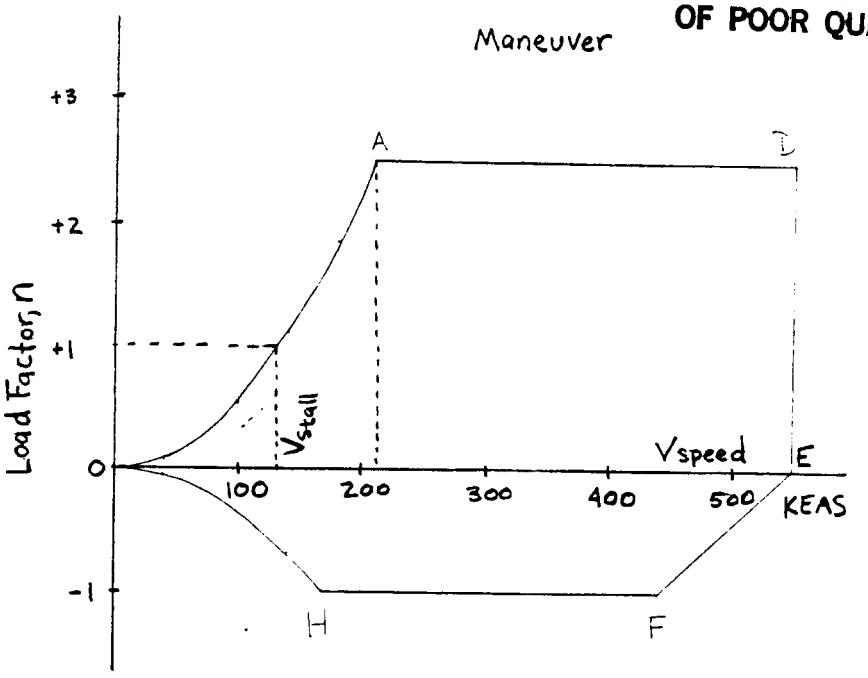

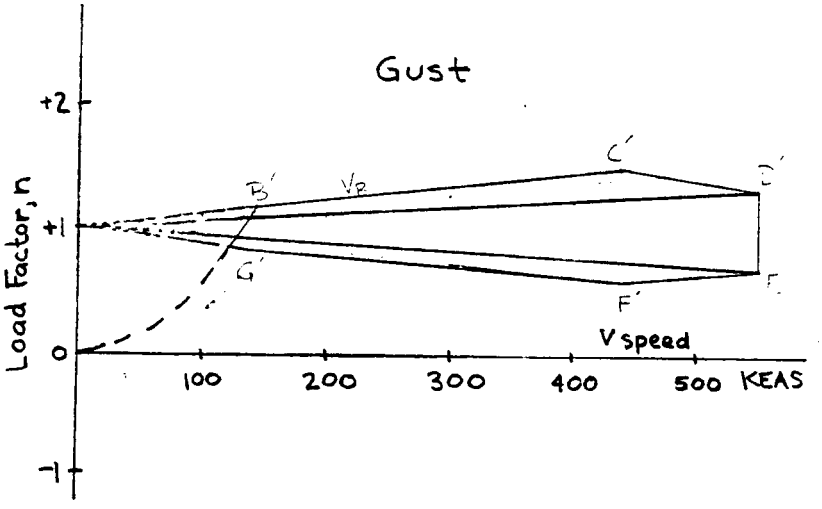

$$V_D = 1.25\, V_C \qquad \text{Eq. 11.4}$$

11. 2 Wing Loading

It was assumed that the wing was subjected to a uniform loadings due to lift and the fuel stored in the wing. It was also assumed that the wing was subjected to a singular load due to the landing gear. To analyze the effects of the loading, the wing was treated as a cantilever beam. The sectional lift coefficient was calculated at five spanwise stations using the vortex-lattice program supplied by Mr. David Poladian of Cal Poly Pomona. An average lift coefficient was determined and a lift distribution was approximated with respect to the total wing area and the dynamic pressure. Equation 11.5 was then integrated numerically to obtain the the wing bending moment about the fuselage reference. This bending moment was calculated to be 2,950,000 lb-ft. With such a large moment, it was decided to use three spars in the wing structure.

12.0 Noise and Pollution

12.1 NOISE

12.1.1 Sonic Boom

Inherent in the mission profile of the High Speed Civil Transport is supersonic flight, and therefore an appraisal of its sonic boom is required. Sonic boom is the name given to the sudden rise and fall of sound pressure resulting from exceeding the speed of sound and is more familiarly associated with high speed aircraft. The change in pressure level comes from the Mach cones emanating from the bow and tail of the airplane. Figure-12.1 shows the bow and tail waves, the typical pressure wave generated near the ground and a possible ear response to the pressure signal. Most of the sonic boom's energy is concentrated in the infrasonic (below 16Hz) range. 1 The maximum increase in atmospheric pressure due to sonic boom is termed the overpressure and is measured in units of pounds-force per square foot or in the typical sound unit, the logarithmic decibel. Another quantity used to describe the sonic boom is its duration measured in seconds or fractions thereof.

12.1.2 Law

FAR 91.55 states that no civil aircraft which is capable of supersonic flight may operate from a United States airport nor may it operate supersonically in U.S. airspace. Landing waivers have been granted to the Concorde which allow it to operate from a few U.S. airports, but still is prohibited from supersonic flight over land. Current HSCT studies being performed by McDonnell Douglas and Boeing aircraft companies assume subsonic flight overland and as little overland travel as possible.2 The only stipulation to allow supersonic flight in FAR 91.55 is if the pilot

NATURE OF THE PROBLEM

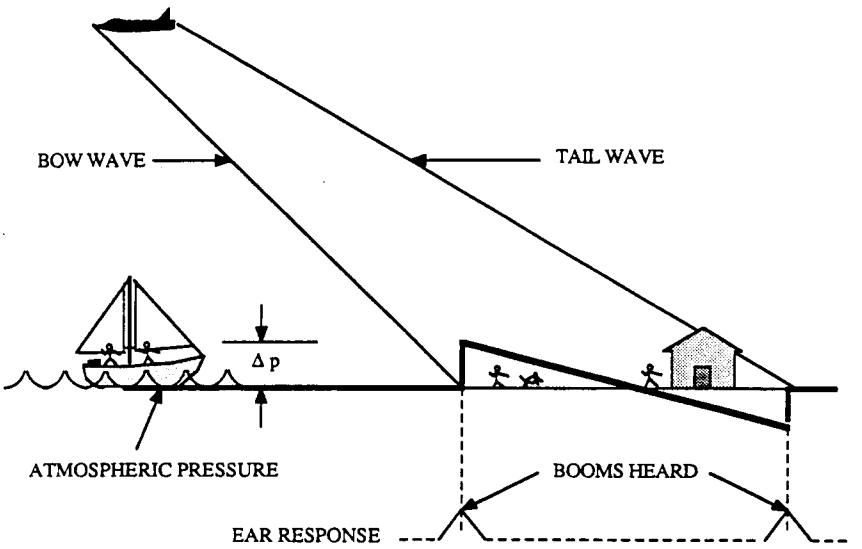

Figure 12.1: The Sonic Boom

is able to determine the sonic boom generated by his aircraft will not reach the ground. It makes no mention of tolerable overpressure levels. The EPA2.5 says there is no public annoyance from 1 daytime (7am to 10pm) ground measured boom below 0.75 psf based on a day-night average of 55 dB, and therefore recommends, for more than 1 boom per day, the peak level of each boom should be less than 0.75/(N)1/2 psf or 125 - log(N) dB where N is the number of booms. It is expected that the attractions and wide ranging benefits of the HSCT will persuade the public to change these laws and instead invoke ones which seek a compromise between feasible operation of an HSCT fleet and sonic boom tolerances.

12.1.3 Prediction Methods

The prediction methods of Carlson[3], Seabass[4] and Morris[5] were compared in estimating the sonic boom signatures produced by the configurations presented in this report. Common to all the methods was input information regarding aircraft shape, speed and altitude.

Morris

Morris' 1960 paper gave the overpressure (dp) as either due to volume effects or lifting effects, whichever is greater. The rise in pressure due to volume was

$$P_V = 0.429\, K_R \sqrt{\frac{P_a}{P_g}}\, K_V\, (M^2\text{-}1)^{0.125}\, \sqrt{S_{AM}}\, l_A^{-0.25} h^{-0.75}\, P_g$$

and the rise in pressure due to lift was

$$P_L = 0.363\, K_R \sqrt{\frac{P_a}{P_g}}\, K_L\, \frac{(M^2\text{-}1)^{0.375}}{M}\, \sqrt{W}\, l_W^{-0.25} P_a^{-0.5} h^{-0.75}\, P_g \quad .$$

The use of this method requires and relies heavily upon an estimate of the volume shape factor KV and the lift shape factor KL which the author states are generally between 1.5 to 2.0 and 1.4 to 1.63, respectively, for "practical supersonic aircraft shapes". KV would be close to 1.5 for bodies whose maximum thickness occur

towards the rear and KL would tend towards 1.63 for shapes similar to delta wings. Morris states that lifting effects will dominate over most of the altitude range of a large bomber or supersonic transport aircraft.

Seabass

Seabass (1972) gave the following equation for the overpressure as

$$P_{so} = \frac{P_g 4e^{\frac{-h}{2H}} l}{3ak\sqrt{2B}\ h}[(1+9/8W')^{1/2} - 1],\quad W' = akBe^{(h/H)(h/l)^{1/2}}\ W/(P_g l^2)$$

$$a = ((\pi)H/(2h))^{1/2}\ \mathrm{erf}(h/(2H))^{1/2}$$

$$k = 2(\text{cap gamma})\ M^2/\text{gamma}\ B(2B)^{1/2}$$

This equation utilizes altitude, length, and speed as the primary parameters but also the atmospheric scale height which was not well defined. He states that the signature shape that is approached asymptotically below the aircraft in an isothermal atmosphere of scale height H is the signature that occurs at a distance (pi)H/2 below the aircraft in a homogeneous atmosphere and the ultimate (pressure signal) advance below the aircraft in a stratified atmosphere is the same as that in a homogeneous atmosphere when z (the distance below the aircraft) = (pi)H/2.

Carlson

Carlson (1978) published a simplified sonic boom prediction procedure which seems the most thorough of the three methods. Carlson employs the combined effects of lift and volume in his effective area equation:

Ae(x) = A(x) + B(x) where B(x) is the equivalent are due to lift and is defined as

A(x) is the cross-sectional area distribution normal to the flight path. Since the aircraft was not assumed to be operating at very large angles of attack, so areas normal to the aircraft longitudinal axis was acceptable. One then calculates a shape

factor assuming a parabolic effective area distribution. Carlson gave proof of the validity of this assumption to calculate the shape factor and its accuracy to within 5% to 10% of the values for current supersonic aircraft using more rigorous computer methods. Like Morris, Carlson employed a reflectivity factor, KR, which one must estimate in order to use the procedure. Morris and Carlson agreed that reflectivity factors between 1.8 for marshy terrain to 2.0 for hard flat surfaces are acceptable. Carlson's model may be used for aircraft altitudes as great as 250,000 ft (76km), ground level altitudes as great as 5200 ft (1600m), aircraft in level flight or in moderate climb or descent flight profiles in the standard atmosphere.

12.1.4 Method Evaluation

Seabass' method gave the lowest overpressures but also required the least information for input. Seabass' equations were only sensitive to length and weight (keeping altitude and Mach constant) and since the four HSCT planforms were within 4% of each other's length and at most 16% different in weight one could expect similar results. The method did not account for aircraft shape or planform which distinguishes the various HSCT configuration to a greater degree than length and weight. Morris' method required more information about the shape of the airplane as given by the boom due to volume factor, boom due to lift factor, wingspan and maximum cross-sectional area inputs. As mentioned above, the volume and lift factors are only estimates therefore the same bias possessed by the person doing the calculations exists in the results. Carlson's method seemed the most planform sensitive of the three procedures being that cross-sectional area and span distributions as well as length, weight, aircraft planform area, and flight track information were required for input. This last method also output the boom time duration, something which the other methods made no mention.

12.1.5 Results

The first method implied overpressures due to lift effects dominate altitudes above 75,000 ft for all Mach numbers for the Blended wing-body. Volume effects were prevalent only at higher Mach numbers and lower altitudes. The second method gave results which were desired but not necessarily probable. Sonic boom overpressures for this method were as low as .87 psf for Mach 1.5 at 35,000 ft altitude and only as high as 1.76 psf for Mach 6.5, 20,000 ft !! A goal of 1 psf for high-speed civil transports has been set in hope that U.S. law-making bodies will accept this ceiling for supersonic flight over land. The second method's results were encouraging that HSCT designs might be able to accomplish their goal. The third method's results were in better agreement with the first's results. Overpressures for the blended wing-body were as great as 8.36 psf for Mach 6, 20,000 ft which seems reasonable from such a large heavy aircraft moving at great speeds at low altitude. Sonic boom decreased as expected at higher altitudes to 1.15 psf, 85,000 ft -- the design point for the blended wing-body. Boom time durations increased with increasing altitude for constant Mach and increased with increasing Mach for constant altitude. Although one would expect that as he flies higher at the same Mach number the time duration should decrease due to atmospheric attenuation the trend was just the opposite, however, as one flies faster at constant altitude the sonic boom grew stronger and lasted longer as predicted.

12.1.6 Trends

McDonnell Douglas HSCT reports for a 600,000 lbf aircraft Mach 4 at 80,000 ft was estimated to produce a 1.0 psf overpressure and a Mach 6 design at 95,000 ft would produce 1.6 psf (approximately). A sonic boom study performed by Driver for a Mach 2.7, 250 passenger 5500 nm conventional delta-wing Concorde-like design (with fuel only for a 2500 nm range) produced 1.45 psf and a proposed low-boom

design (arrow-head shaped) would produce 0.72 psf at cruise conditions. Driver's study indicated the use of planform and cross-sectional area distributions like that of Carlson.

Current supersonic aircraft have been measured to produce overpressures as much as 98 dB (3.1 psf)3 whereas the point at which humans experience pain to their unaided ear is about 134 dB (210 psf)6. One should keep in mind that sonic booms are generally within 100 to 500 milliseconds in duration1 and their effect on humans is only a startle. However, sonic booms will not only touch humans but also buildings and animals as well.

12.2 Other Sources of Noise

12.2.1 Engine

The design of any airplane requires a look at the production of noise from its engines. Noise, in any context, is characterized by its sound level, frequency spectrum, and its variation over time. Sound level refers to the listener's subjective conception of loudness and is a function of the magnitude of pressure fluctuations about the ambient barometric pressure.9.5 As the HSCT configuration of this report was employing an air-turbo ramjet, an unconventional engine and noise generators and suppressor techniques were considered. Acoustic liners to act as the inner skin of the engine fairing in parts throughout the entire engine are, in general, effective sound absorbers. In some cases they have reduced noise by 10dB10 but encountered operational problems like freeze-thaw transition and fuel/oil retention. for those and other reasons alternative reduction methods for unique stages of the engine must be considered.

12.2.2 Inlet

Coming from the inlet system of an aircraft engine is noise from the compressor, which is most prominent during the approach phase. This noise is characterized by two types -- broad-band and discrete tone noise. Broad-band noise is turned by the turbulence and flow velocity as it enters and is generated by the compressor blades. The acoustic energy from the turbulent flow is proportional to its velocity to the 5th power. The incidence angles of the compressor blades also play a key role in noise production. A one degree divergence of blade incidence angle from the optimum angle can increase noise by 3 dB. Discrete tones are associated with the fans of low- or high-bypass ratio turbofans but can also occur from compressor stages. When the supersonic tips of blades have shock waves that are not identical the familiar buzzsaw noise is produced but also the cyclic pressure field and wake interactions which exist between rotating and stationary stages are a cause of discrete tones. The correct spacing of the compressor stages and blade sweep-back to defeat the shock problem have been noted as possible solutions. Also proposed is the introduction of an hemispherical honey-comb skin inflow control device to mount in front of the inlet during the landing and approach phases. This device was tested on conventional turbofan engines.11 A couple of the key factors in helping reduce the internal noise of a 2-stage turbo fan by 20 dB in addition to the ideas presented above was the elimination of inlet guide vanes, divided or non-circular intakes and introduction of acoustic insulation.10

12.2.3 Combustor

Noise emanating from the combustor region has been difficult to isolate and little is known about it. One item which is known is that combustors generate low frequency noise and is less annoying than the high frequency buzzsaw whine of the compressor and/or fan.

12.2.4 Turbine

Broad-band and discrete tones are also present in this stage of the engine. To combat these a lesser ratio of stationary to rotating blades than in the fan should be used due to the lower Mach number of the hot flow. High blade loading should be avoided. Large stage spacing is recommended.

12.2.5 Jet

Jet noise is probably the most prominent of all engine noise sources especially during the takeoff phase. Key factors here are exhaust flow velocity and temperature profiles. Early civilian turbojet engines such as the ones used on early DC-8's were loud due to the flow of high temperature, high velocity exhaust gases. The popularity of the high-bypass ratio turbo fan grew not only from its lower fuel consumption but also from its quieter exhaust. The idea was (and still is) to surround the hot jet core with cool bypass air. The problem, though, of the hot jet core still exists. One way to combat this problem is to use an inverted-velocity-profile (IVP) coannular jet which has the hot flow at high speed but over a greater area surrounding the low temperature, low speed flow. The hot core which was once a concentrated flow is now disbursed to the atmosphere at a higher rate thus quieting the exhaust. Other suppression techniques include ejectors, thermo-acoustic shields, mechanical chute suppressors and advanced operational procedures, the latter to be discussed later. The concept behind mechanical suppressors is they slow the jet flow as close to the nozzle as possible such that the shear between exhaust flow and atmospheric air is minimized. The thermo-acoustic shields act as heat and sound energy absorbers and reflectors, respectively. The exhaust temperatures are decreased and sound energy is reflected away from the ground rather than towards it. Ejectors create another path of exit for exhaust and

thus have mixing characteristics like the IVP coannular jet. In the past, the weight, cost and drag penalties of ejectors have eliminated them from widespread usage but the takeoff thrust required and the associated airport noise will probably take priority.

12.3 Regulations

FAR 36, Appendix C, Section 36.5 gives the maximum noise levels for various types of aircraft for takeoff, approach, sideline and landing conditions. The measurement stations are given as:

takeoff: 21325 ft from the start of the takeoff roll on the extended centerline of the runway.

approach: at a point 6562 feet from the threshold on the extended cneterline of the runway.

sideline: on a line parallel to and 1476 feet from the extended centerline where the noise level after lift off is greatest or 0.35 nm for three or more turbojet engines with Stage 2 levels.

landing: 1.08 nm from point where the aircraft could clear a 50 ft obstacle on the extended centerline of the runway.

These measurement points can be visualized with the help of Figure-12.2. The "Stage" level is a function of the takeoff weight as seen in Figure-12.3. The maximum takeoff weights of any of the HSCT planforms, including the blended wing-body, coincide with the 108 EPNdB FAR requirement. EPNdB is an acronym for Equivalent Perceived Noise level which takes into account the sensitivity of the human ear to frequency and tone annoyance, together with the duration of exposure to the noise. In California, the home of major international airports likely to serve the HSCT, the CNEL shall not exceed 65 dBA at airports' property

FAA NOISE - MEASURING POINTS

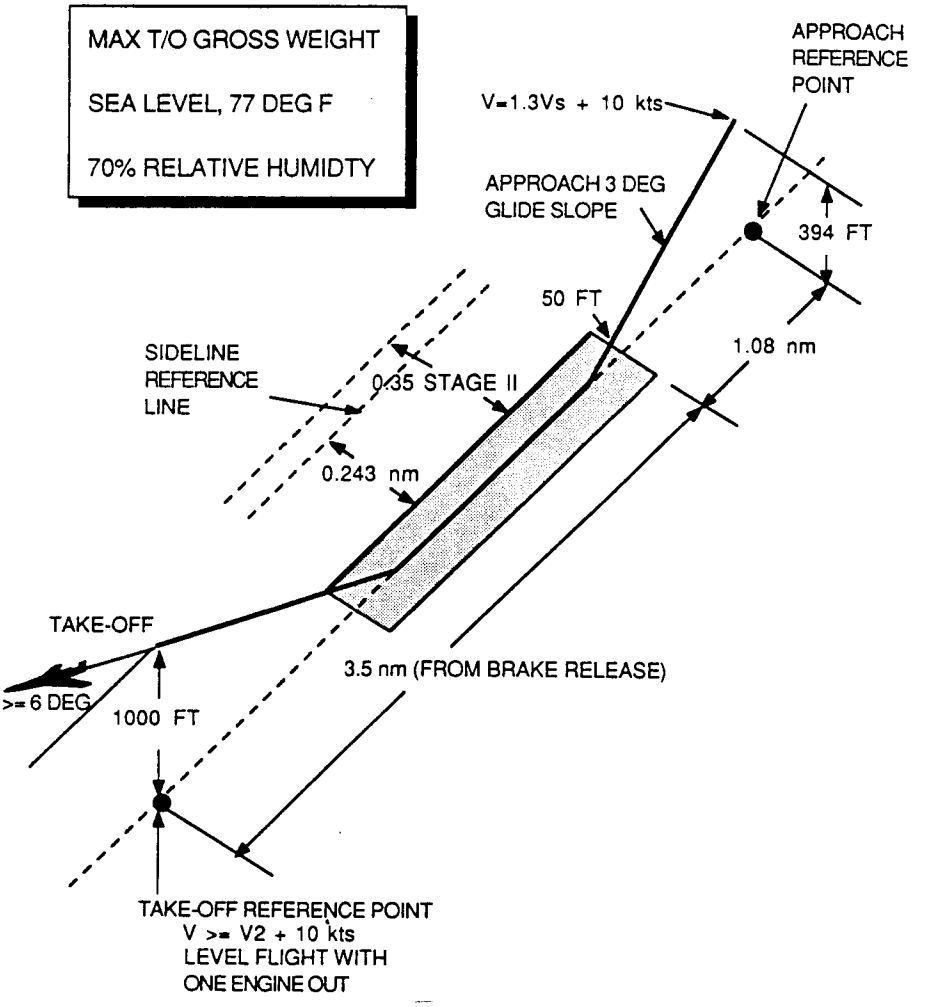

Figure12.2

boundaries.1 CNEL is the acronym for Community Noise Equivalent Level which is a noise rating method using an average level which exceeds a threshold value and is integrated over 24 hours.15 FAR36 gives exception to Concorde making its guidelines Stage 2 rather than the quieter Stage 3 and states: "...noise levels of the airplane are (or should be) reduced to the lowest levels that are economically, reasonable, technologically practicable, and appropriate for the Concorde type design." This statement translates into a proposition that if supersonic transport or HSCT manufacturers/designers reduce noise levels as much as possible then exemptions and/or exceptions to the law might apply.

12.3.1 Trends

Figures 12.4, 12.5, and 12.6 show noise levels for many commercial aircraft in the modes of approach, takeoff and sideline to familiarize the reader with the current trends in meeting or exceeding FAR requirements. One notices Concorde's noise as being louder than all other aircraft on the figures. Reference 14 says "experience at London, Washington and New York suggests that it (Concorde) is not as annoying to the public as one might think. Certainly complaints levelled specifically against Concorde have dropped dramatically at all three airports once the novelty has worn off. At New York in particular the local inhabitants seemed to have been surprised when the aircraft was eventually allowed in, that Concorde in general caused them less annoyance than other aircraft which had been operating without hindrance."! Conflicting with that report is a statement made by an Ontario Airport official who said that after the Concorde landed there once it was then restricted on the basis of its noise output from landing at Ontario again.16

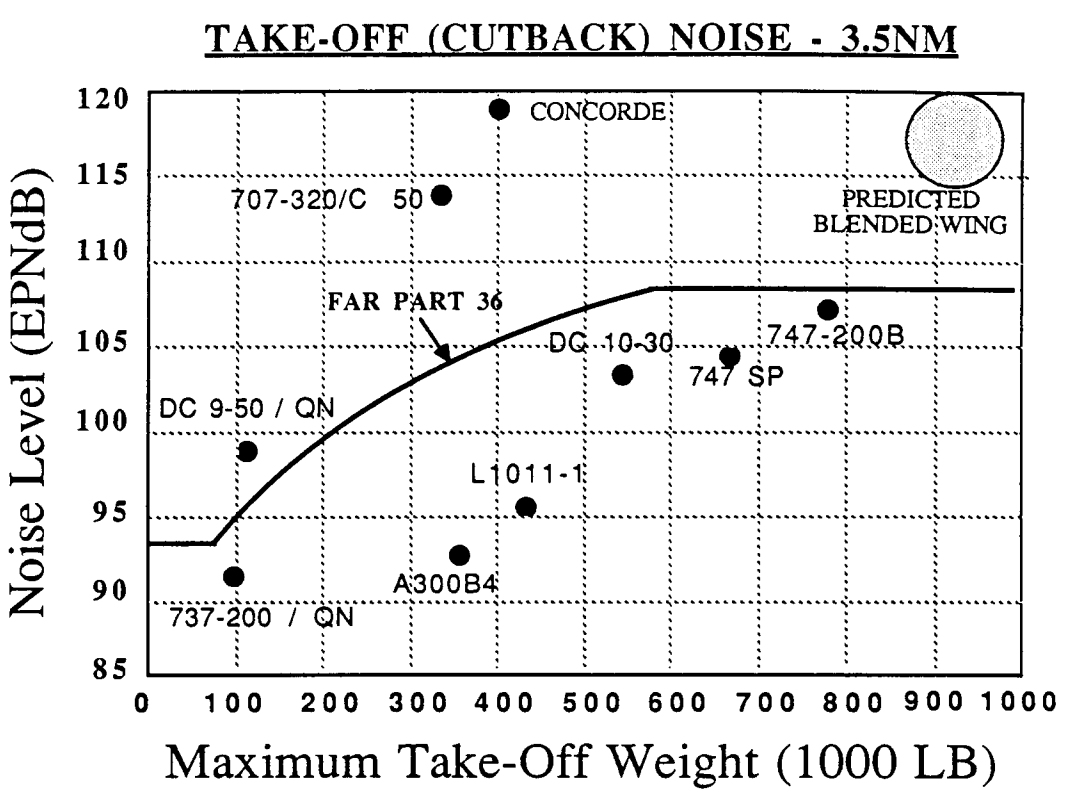

Figure12.3

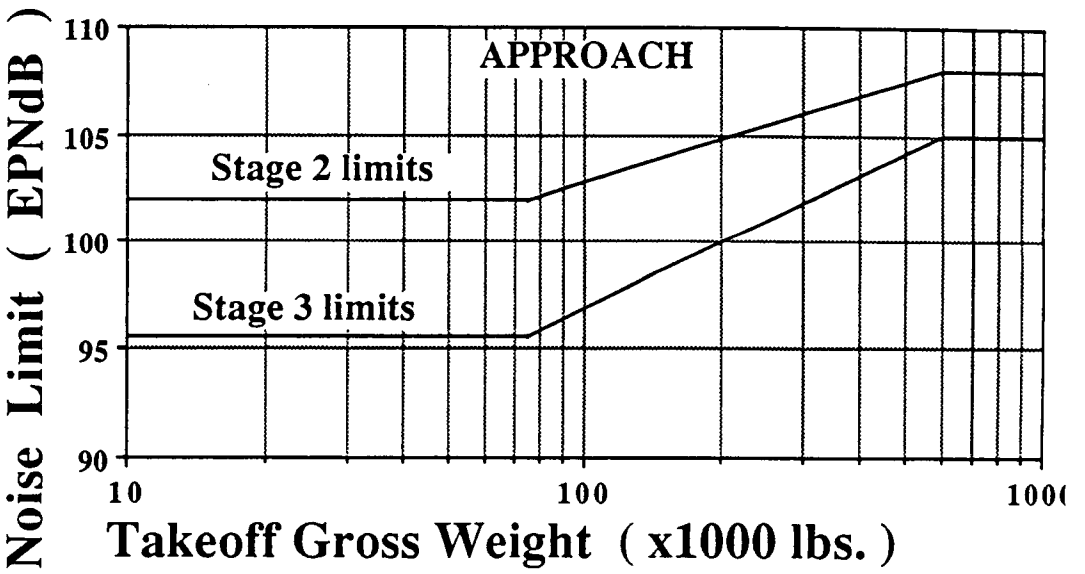

Figure12.4

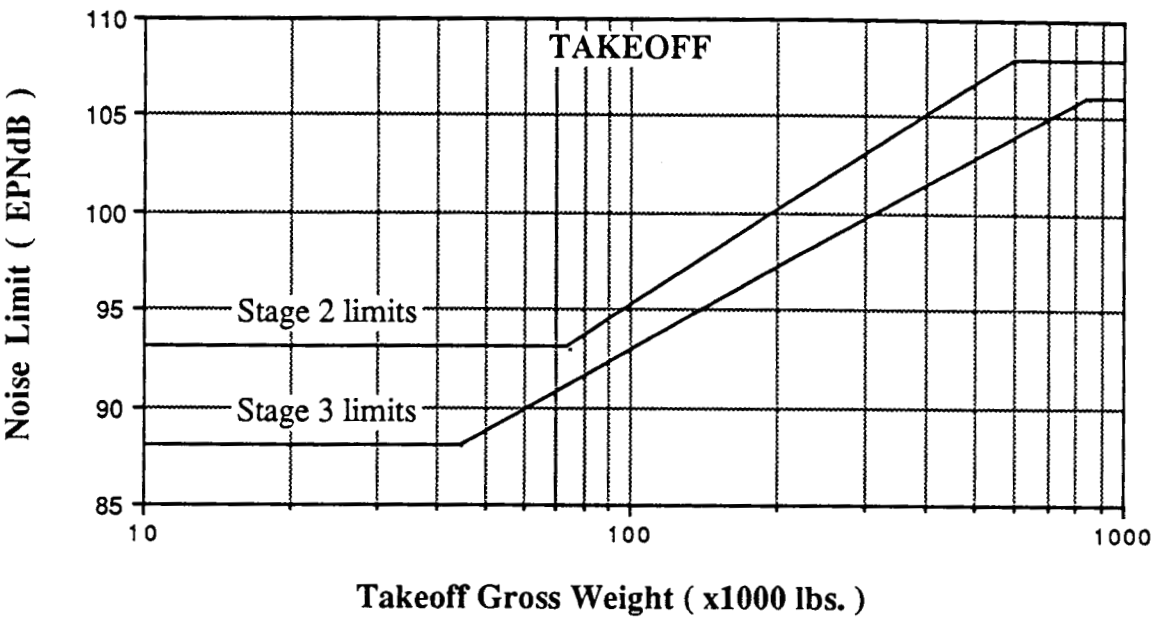

Figure12.5

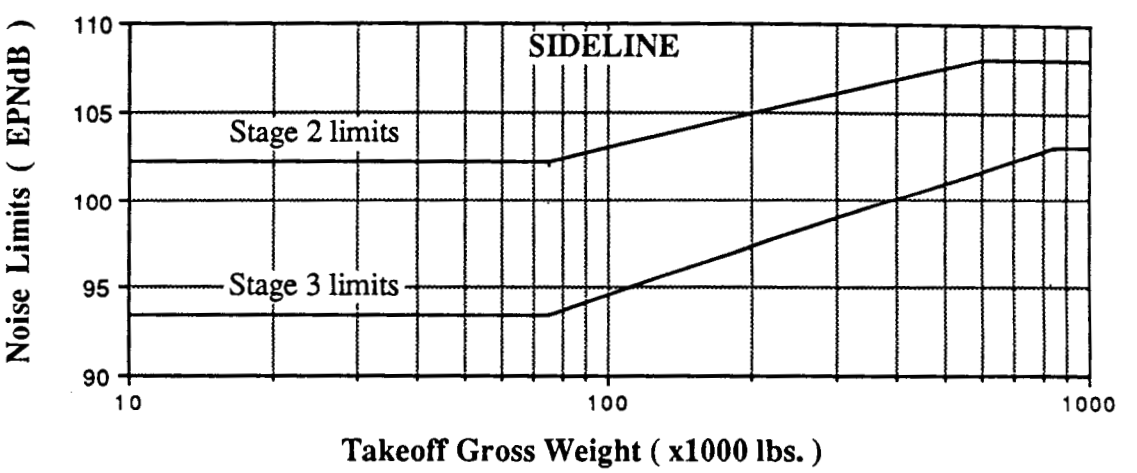

Figure12.6

12.3.2 Airport Noise Reduction

A 1982 NASA study17 of a Mach 2.62, blended-wing, 290 passenger, 4423 nm range transport concept reduced takeoff noise emissions from 105.7 EPNdB to 103.4 EPNdB using advanced takeoff operations. These tests were performed assuming the use of four double bypass VCE engines with IVP nozzles and 20-chute suppressors. The advanced procedure which had the greatest reduction in sideline noise had the following features: 1) a rotation speed at 200 knots (vs 185 standard), 2) a climb speed of 250 knots (vs 223), 3) stepped flap settings from 20 degrees to 10 degrees at V2 (vs constants 20 degrees) and 4) autothrottle setting from 100% to 84% thrust at V2 and then to 41% thrust 18,000 ft from brake release. A graphical of this procedure can be seen in Figure-12.7. The climbout is essentially constant at an angle of 2 degrees. The significance of this advanced procedure lies in the cutback of thrust to noise-crucial yet safe levels during the climbout. This procedure produced the smallest 108 EPNdB and 104 EPNdB countour areas of 0.82 and 1.25 square nautical miles, respectively. The best landing approach by this report was one of a 6 degree glide slope with net thrust held at approximately 15% until the thresholed of the runway versus the standard 3 degrees slope at a 20% power setting. Even though these numbers may not be valid for the Joined wing HSCT there are lessons to be learned. A stepped thrust profile on takeoff and a stepp glide slope on approach, if deemed saife as were the profiles in the NASA study, are highly recommended.

12.4 Pollution

Methane is what is termed an alkaline or paraffin. It constitutes 50 to 90% of natural gas. Incomplete combustions of methane yields carbon black which is used in rubber compounding and printing ink. Oxygen deficient burning of methane produces carbon monoxide and when heated above 9000 C it converts or dissociates

to its carbon and hydrogen components. The reaction of methane with oxygen produces carbon dioxide and water in the balanced equation:

$$CH_4 + \frac{3}{2}O_2 \quad >>> \quad CO_2 + 2H_2O \quad .$$

Combustion in air, however, yields the usual carbon monoxide, hydrocarbons, nitric oxides, sulfur oxides (depending on the sulfur content of the fuel) and particulates.

It has been suggested that a fleet of supersonic transports operating at high altitudes would effect the ozone layer. One article20 recommended that such a fleet should operate above 95,000 ft as the 80,000 ft to 95,000 ft layer containes ample free oxygen to provide stability to the 65,000 ft to 80,000 ft layer which varies in quantity of free oxygen atoms -- one of the key factors to the reformation of ozone. Minimal ozone, however, resides in the 80,000 ft to 85,000 ft. If the exhaust emissions of the Joined wing HSCT deplete ozone then it would be advantageous to fly in a region where there exists the least amount of ozone. Figure-12.8 shows an approximate distribution of ozone in our atmosphere. Some attention might be paid to weather patterns and seasons since Johnson of reference 21 states that ozone concentrations are 10% lower than normal before a storm and 20% higher than normal after a storm. He also states that concentrations are greatest at the high latitudes in Spring.

Emission standards for SST as of 1979 for new manufactured models were 3.9, 30.1 and 9.0 pounds hycrocarbon, carbon monoxide and nitric oxides per 1000 pound thrust per cycle, respectively15. Beheim23 and Petrash11 said that hydrocarbons and carbon monoxide were the dominant emissions at idle conditions where oxides of nitrogen and smoke were dominant at takeoff. Petrash11 suggests to increase the burning zone, increase the residence time by reducing the flow velocity or by delayed mixing, add more fuel to the fire to raise local temperature and improve

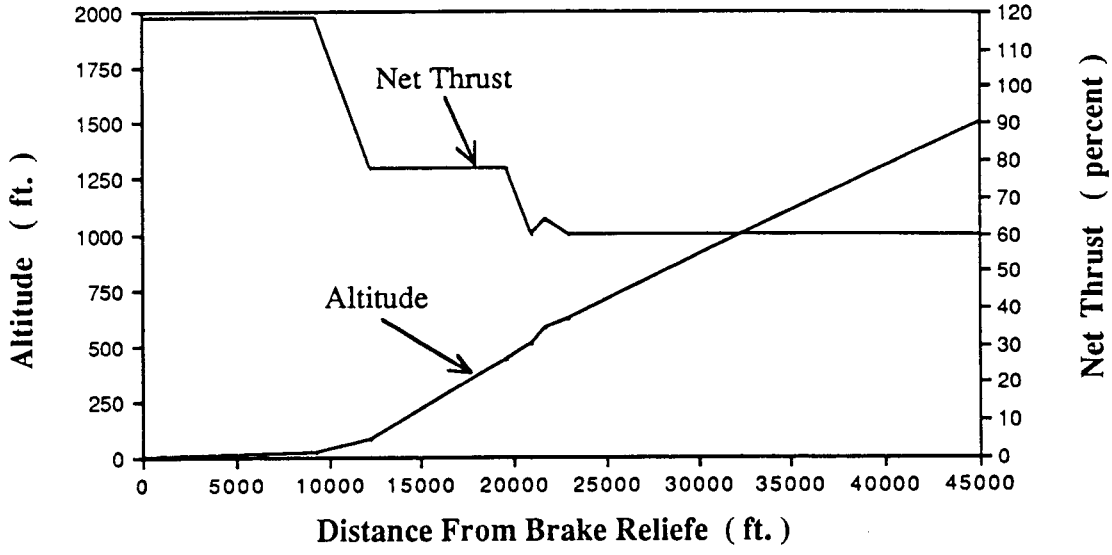

Figure - Advanced Takeoff Procedure

Figure12.7

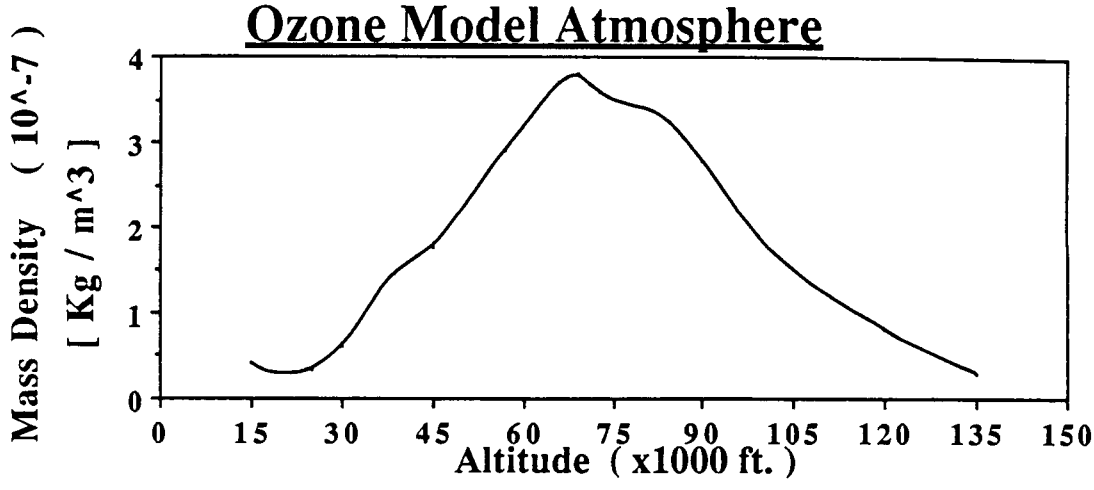

Figure12.8 Ozone Model Atmosphere

fuel atomization to burn lean will reduce idle emission of HC and CO. Running fuel lean, enhancing mixing, increasing flow velocity and again better fuel atomization will reduce the NOx and smoke emission dominating the cruise or high power regimes. The combustor characteristic were realized in the Vorbix combustor of a JT9-D engine. CO was reduced by about 50%, HC was reduced by a factor of 10% and oxides of Nitrogen by 35%. Catalyzed combustion was also suggested as it aided in nearly pollutant-free combustion.

An article opposed the beliefs of many texts which had proof nitric oxides did not affect ozone. A study done in the early '60's of nuclear tests revealed that the large quantity of nitric oxide created from a total of some 340 megatons of nuclear explosions over a four year period showed no evidence of any decrease of any decrease in ozone. Such a large quantity of NOx would be "perhaps three times that of upper estimates predicted from 500 SSTs flying 7 hr. a day for a year." 22 stations in the Arctic and 2 stations in the Antarctic recording 12,000 ft altitude nuclear detonation activity during the years of 1961 and 1962. Nuclear explosions were also made in the Pacific at equatorial latitudes where introduction of large concentrations of NOx with sunlight are suppose to be even more contributory to catalytic ozone reduction.

13.0 ECONOMICS

13.1 Introduction

As subsonic travel is loosing its ability to keep up with the pace and needs of today's traveler, the modern and future business person will turn towards ever faster and efficient means of transportation. Concorde sought to fill this need but with current trans-Atlantic fares of $5,500, its inability to fly into many U.S. airports because of noise and intolerable sonic boom overland, Concorde has not found its niche. Responding to the demand will be the Joined wing HSCT, however, if the monetary risks of building such an airplane are too high, as was the case with the early 1970's U.S. SST, the program will die. It is the objective of this section to examine the costs and feasibility of the blended wing-body.

13.2 Airframe Cost Evaluation

The cost estimation was done with a paper published by the Rand Corporation**. The report was the result of the reduction of cost data on post World War II cargo, tanker, fighter, bomber and trainer aircraft as well as aircraft in the 1970 era -- A-7, F111-A, C141 and OV-10. These aircraft were composed mostly of aluminum alloy, 5000 to 113,000 lbf in AMPR weight (to be described later) and had maximum speeds of Mach 0.5 to Mach 2.2. The method outputs development and production costs of aircraft airframes and subsystems such as engines and avionics, in a long-range planning context.

13.3 Limitations and Inclusions

The Development phase was defined as the nonrecurring manufacturing effort undertaken in support of engineering. It includes manufacturing labor, material for mock-ups, test parts and static test items. Development costs of, say, M aircraft include development support, flight test operations and cumulative cost of M flight test aircraft plun N operational aircraft. Test facilities nor manurfacturing facilities were included. Flight test operations cost includes costs incurred by the contractor to carry out flight tests, engineering, planning, data reduction, manufacturing support, instrumentation, spares, fuel, oil, pilots, facilities and insurance. Tooling costs encompass tool design, planning, fabrication, production of test equipment, maintenance of tooling, production planning and various changes which might take place during the production phase. Material costs include that for raw material, hardware and purchased parts for the major structure. The method decreases material cost per lbf of aircraft with quantity produced due to a built-in learning curve. Prototype costs cover limited tooling, few test articles, off-the-shelf engines and avionics but do not furnish production planning. Avionics costs, like materials, have a learning curve associated with it. One of the paper's disclaimers stated, "It is emphasized that far greater uncertainty exists when the (cost) equations are applied to aircraft whose technological or performace characteristics are outside the range of the sample." Clearly the blended wing-body HSCT planform, like the other planforms of the overall study, lie outside the range of the sample therefore, great uncertainty will plague calculations done for the HSCT.

C-2

13.4 Other Factors

Another study of HSCTs done by Douglas aircraft18 examined some of the other economic aspects such as market analysis, utilization, fuel and vehicle worth. Market analysis yielded expectations that by the year 2000, the Pacific Basin will exceed the European Economic Community by 0.8% in economic growth while the North/mid-Pacific and North Atlantic markets will represent two-thirds of the total world international traffic. HSCT will accomodate these regions since routes in these regions have trip distances of 6,000 to 7,500 miles and since Mach 5.3 travel such as that of the blended wing-body will cut 7,500 mile trip time from 14.4 hours to 3.7 hours. Mach 5.3 cruise also sees benefits in utilization. The change in annual seat-miles per aircraft with Mach number tends to its minimum value at Mach 4 where annual seat-miles per aircraft are at about 1,800. Douglas' report states, "Of all the (cost) elements, fuel represents the most significant cost driver." The acquisition of methane was seen to be projected as euqal to that of Jet A fuel, each costing 10 cents per pound, but only methane would be able to deliver the performance necessary at Mach 5 cruise. In terms of vehicle worth, or in other words passenger revenue, direct and indirect operating costs and a 10% return on investment to the operator, Mach 5 LNG-fueled HSCTs produce vehicle worths 200% greater than advanced subsonic transports but also have the greatest sensitivity towards change in fuel price -- "a 1 cent per gallon change in methane...results in a $2.3 million change in vehicle worth." What could save the day for HSCTs would be if turn-around times were 1 hour, for such a time would generate $75 million in additional vehicle worth according to the Douglas report.

REFERENCES

1. Roskam, Jan. Airplane Flight Dynamics, Part 1. Kansas: Roskam Corp., 1978.

2. Nicolai, Leland M. Fundamentals of Aircraft Design. California: Mets, Inc., 1984.

3. "Aircraft Synthesis" ACSYNT, NASA Design Program

4. Ellison, D.E., USAF Stability and Control Handbook (DATCOM). Ohio: AF Flight Dynamics Lab, AFFDL/FDCC, Wright-Patterson AFB, 1969.

5. Truitt, Robert W. Hypersonic Aerodynamics. New York: The Ronald Press Co., 1959.

6. Truitt, Robert W. Fundamentals of Aerodynamic Heating. New York: The Ronald Press Co., 1960.

7. Detra, R.W. and N.H. Kemp and F.R. Riddell. Addendum to "Heat Transfer to Satellite Vehicles Re-entering the Atmosphere". California: ARS Jet Propulsion, 1957. p.1256 6.

8. Davey, Robert F., Supplementary Notes to Airrcraft Engines and Gas Tubines,, California Polytechnic University, Pomona, 1985.

9. Dusa, D. J. High Mach Propulsion System Installation and Exhaust System Design Consideration , AIAA-87-2941, Sept. 1987.

10. Whitlow, John B., Jr.; Eisenberg, Joseph D; Shovlin, Michael D., Potential of Liquid-Methane Fuel for Mach 3 Commercial Supersonic Transports , NASA TN D-3471, 1966.

11. CRC Handbook of Tables for Applied Engineering Science, 2nd ed. Eds. Ray E. Bolz, D.Eng., and George L. Tuve, Sc.D. Ohio: CRC Press, 1973.

12. Ames Research Staff, Equations, Tables, and Charts for Compressible Flow , NACA Re-1135, 1953.

13. Seddon, J.; Goldsmith, E. L., Intake Aerodynamics , Collins Professional and Technical Books, Great Britain, 1985.

14. Pace, Steven. North American Valkyrie XB-70. California: Aero Publishers, Inc., 1984.

15. Miller, Jay. Convair B-58. Texas: Aerofax, Inc., 1985.